Divergent changes in aerosol optical hygroscopicity and new particle

2	formation during a heatwave of summer 2022
3	
4	Yuhang Hao ^{1, a} , Peizhao Li ^{1, a} , Yafeng Gou ¹ , Zhenshuai Wang ¹ , Mi Tian ¹ , Yang Chen ² ,
5	Ye Kuang ³ , Hanbing Xu ⁴ , Fenglian Wan ¹ , Yuqian Luo ¹ , Wei Huang ⁵ , Jing Chen ^{1, 6, *}
6	
7	¹ College of Environment and Ecology, Chongqing University, Chongqing 400045,
8	China
9	² Center for the Atmospheric Environment Research, Chongqing Institute of Green
10	and Intelligent Technology, Chinese Academy of Sciences, Chongqing 400714, China
11	³ Institute for Environmental and Climate Research, Jinan University, Guangzhou
12	511443, China
13	⁴ Experimental Teaching Center, Sun Yat-sen University, Guangzhou 510275, China
14	⁵ National Meteorological Center, China Meteorological Administration, Beijing
15	100081, China
16	⁶ Key Laboratory of Three Gorges Reservoir Region's Eco-Environment, Ministry of
17	Education, Chongqing University, Chongqing 400045, China
18	
19	^a These authors contributed equally
20	Courses and area to line Chan (shop iing@agu adu an)
21	Correspondence to: Jing Chen (chen.jing@cqu.edu.cn)

Abstract. As a crucial climate-forcing driver, the aerosol optical enhancement factor (f(RH)) is significantly modulated by chemical compositions and the evolution of particle number size distribution (PNSD), e.g., during new particle formation (NPF). However, the mechanisms regulating aerosol optical hygroscopicity during different NPF days, particularly those influenced byunder heatwaves due to global warming, remain poorly understood. In the 2022extremely hot summer of 2022 in urban Chongqing of southwest China, simultaneous measurements of aerosol optical and hygroscopic properties, PNSD, and bulk chemical compositions were conducted. Two distinct types of NPF were identified: the ones with relatively polluted period (NPF_{polluted}) and clean cases during heatwave-dominated period (NPF_{clean, HW}). Compared to the NPF_{polluted} events, NPF_{clean, HW} occurred approximately one hour earlier and the subsequent growth was prolonged, accompanied by a smaller aerosol effective radius (Reff) and lower formation/growth rate during heatwaves. This agreed with the concurrently increased aerosol hemispheric backscattering fraction and scattering Ångström exponent. A generally higher f(RH) was observed generally higher on NPF days in comparison tothan that for non-event cases in both periods, partly attributed to distinct changes in PNSD patterns during NPF days. Moreover, heatwave-induced stronger photooxidation may intensify the formation of more hygroscopic secondary components, as well as and prolong the atmospheric aging/subsequent growth of both pre-existing and newly formed particles, largely contributing to thereby enhancing the enhanced f(RH) especially during NPF_{clean, HW} days. The promotedhigher f(RH) and lowered R_{eff} could synergistically elevate the aerosol direct radiative forcing, specifically under persistent heatwave conditions. Further in-depth exploration on molecular-level characterizations and aerosol radiative impacts of both direct and indirect interactions under heatwaves and other weather extremes with the warming climate are recommended.

48

22

23

24

25

26

27

28

29

30

31

32

33

34

35

36

37

38

39

40

41

42

43

44

45

46

1 Introduction

49

50 Weather extremes (e.g., heatwaves) have become more and more frequent and intense largely due to the global climate change, and the heatwave-driven 51 environmental, climatic, and health effects have garnered widespread attention 52 (Hauser et al., 2016; Sun et al., 2016). The China Climate Bulletin 2022 confirmed 53 that the national average temperature reached an unprecedented high level since 2012 54 55 (China Meteorological Administration, 2022), and the risk of heatwaves in China will persist and potentially intensify in the future (Guo et al., 2016; Li et al., 2017). 56 57 Extreme heatwave events could pose significant threats to human health, the survival of organisms, agriculture, and socio-economic activities (e.g., power supply 58 restrictions) (Anderson and Bell, 2011; Ma et al., 2021; Su, 2021). Moreover, 59 60 heatwaves can trigger natural disasters such as droughts and wildfires, affecting social stability (Sharma and Mujumdar, 2017). 61 Heatwayes could also affect the atmospheric physical and chemical processes by 62 63 modulating ambient meteorological conditions. Specifically, extremely high temperature weather is typically characterized by a combination of intensified solar 64 radiation with elevated temperature and low humidity levels. This could significantly 65 affect the formation and evolution of secondary aerosols in the atmosphere (Bousiotis 66 et al., 2021; Hamed et al., 2011; Kurtén et al., 2007), given that the air temperature is 67 crucial for chemical reactions (Xu et al., 2011). New particle formation (NPF) serves 68 69 as a crucial source of atmospheric particulate matter and plays a significant role in the secondary transformation processes in the atmosphere (Zhu et al., 2021). Generally, 70 NPF involves the initial formation of thermodynamically stable clusters from 71 condensable vapors (e.g., ammonia, sulfuric acid, and organic precursor gases) and 72 73 subsequent growth of the formed clusters, eventually reaching detectable sizes or even larger dimensions (Kerminen et al., 2018; Kulmala et al., 2003, 2012). Over time, 74 these newly formed particles have the potential to serve as cloud condensation nuclei 75 76 (CCN), thereby impacting the global climate (Salma et al., 2016). NPF events normally introduce a sharp increase in the number concentration of nucleation mode 77

particles within a short time, altering the particle number size distribution (PNSD).

These variations in PNSD likely influence intrinsic physicochemical properties of

aerosols, such as the optical hygroscopicity (Chen et al., 2014; Titos et al., 2016; Zhao

81 et al., 2019).

80

82

83

84

85

86

87

88

89

90

91

92

93

94

95

96

97

98

99

100

101

102

103

104

105

106

107

Aerosol hygroscopicity plays a critical role in the atmospheric environment and climate change, given the complex interaction between aerosol particles and water vapor (Zhao et al., 2019; Zieger et al., 2011). Water uptake by aerosols not only alters the particle size and composition (e.g., as reflected in the aerosol refractive index) but also impacts aerosol scattering efficiency, which further contributes to the uncertainty in aerosol radiative forcing estimation (Titos et al., 2016, 2021). The aerosol optical hygroscopicity parameter, f(RH), defined as the ratio of the scattering coefficient at a certain RH to that of the dry condition, was widely used to describe the aerosol scattering enhancement through water uptake (Covert et al., 1972; Titos et al., 2016; Zhao et al., 2019). Numerous studies have demonstrated that f(RH) is influenced by the size distribution, in addition to particle chemical composition (Chen et al., 2014; Kuang et al., 2017; Petters and Kreidenweis, 2007; Quinn et al., 2005). There is currently limited research on the variations in aerosol optical hygroscopicity during NPF days despite significant changes in aerosol size distributions and chemical compositions, partly due to that newly formed particles insignificantly affect the optical properties of aerosols (Kuang et al., 2018). However, previous studies have observed the enhancement in aerosol hygroscopicity (Cheung et al., 2020; Wu et al., 2015, 2016) and extinction coefficients (Shen et al., 2011; Sun et al., 2024) during the subsequent growth of NPF. It is suggested that the influence of NPF on aerosol hygroscopicity was likely due to changes in aerosol chemical composition at different stages of NPF events (Cheung et al., 2020), whereas the subsequent particle growth associated with NPF events can significantly affect particle hygroscopicity as well (Wu et al., 2016). Although previous studies showed the dependences of aerosol hygroscopicity on chemical composition (Petters and Kreidenweis, 2007; Titos et al., 2016; Zhao et al., 2019) (e.g., the variation in composition of precursor species during NPF events), it is important to acknowledge that the utilized chemical compositions of NPF were either from PM_{2.5} or PM₁ bulk data. This may differ from the corresponding composition of newly formed ultrafine particles primarily in the nucleation and Aitken modes, further introducing bias in exploring the impacts of NPF and subsequent growth on aerosol optical hygroscopicity. Hence, more comprehensive investigations on the influencing mechanisms of aerosol optical hygroscopicity from different perspectives are required, e.g., for the aspects of the evolution of particle size distribution in modulating aerosol optical and hygroscopic properties (Tang et al., 2019; Zhao et al., 2019). Additionally, field observations on *f*(RH) under extreme weather conditions (e.g., heatwaves) are rather scarce, largely hindering our understanding of how weather extremes (e.g., extremely high temperature) influence the optical hygroscopic properties of aerosols. This knowledge gap further impedes comprehensive understanding of the aerosol water uptake property and resulted effects on air quality and the climate under varied synoptic conditions.

During the summer of 2022, a rare heatwave event raged throughout China, especially the Sichuan-Chongqing region of southwest China (Chen et al., 2024; Wang et al., 2024), with the daily maximum temperature exceeding 40 °C lasted for 29 days observed at Beibei meteorological station in Chongqing (Hao et al., 2023). This persistent heatwave not only impacted residents' daily lives significantly, but also affected the aerosol optical and hygroscopic properties likely through changed aerosol physicochemical characteristics and relevant atmospheric processing during the period. In this study, a field observation was conducted by using a combination of a home-built humidified nephelometer system and a scanning mobility particle sizer (SMPS), along with the total suspended particle (TSP) filter sampling. A main goal of this study is to investigate the influence of heatwaves on both aerosol optical hygroscopicity and the NPF with subsequent growth events, along with the related discrepancies. Furthermore, we aimed to explore the mechanisms behind the variability in f(RH) under different meteorological conditions and diverse NPF events. This study will further enrich insights into the potential environmental impacts due to

variations in the aerosol optical hygroscopicity and size distribution, specifically under heatwaves with the changing climate.

139

140

141

142

143

144

145

146

147

148

149

150

151

152

153

154

155

156

157

158

159

160

161

162

163

137

138

2 Data and Methods

2.1 Field observation

A continuous field observation on aerosol optical, hygroscopic and chemical properties was carried out from July 29 to August 19, 2022. The detailed description of the observation site is available in Supporting Information, S1. During the observation period, urban Chongqing suffered a rare heatwave (Fig. S1; Chen et al., 2024; Wang et al., 2024), which significantly affected the local transportation and industrial activities (Hao et al., 2023). China Meteorological Administration (CMA) defines heatwaves as three or more consecutive days with daily maximum temperature (T_{max}) above 35 °C (http://www.cmastd.cn/standardView.jspx?id=2103; Guo et al., 2016; Sun et al., 2014; Tan et al., 2007). Since no unified definition of heatwaves worldwide, the whole study period was categorized into two stages according to CMA's criteria of the daily T_{max} records and the Excess Heat Factor (EHF) metric proposed by Nairn and Fawcett (2014) (Fig. S2a): (1) the normally hot period from 29 July to 6 August (marked as P1); (2) the heatwave-dominated period from August 7-19 (marked as P2) characterized with the consistently occurrence of T_{max} exceeding 38 °C (approximately the last 25^{th} percentile of temperature records for the whole observation period; Fig. S2b).

2.2 Instrumentation and methods

2.2.1 Measurements of aerosol optical hygroscopicity

The humidified nephelometer system, consisting of two three-wavelength (i.e., 450, 525, and 635 nm) nephelometers (Model Aurora 3000, Ecotech Inc.) and a humidification unit, was used to determine the aerosol light scattering enhancement factor, *f*(RH). Ambient air was firstly dried through a Nafion dryer (model MD-700,

Perma Pure LLC) to ensure RH <35%, then split into two streams for both dry and humidified nephelometers operated in parallel. The flowrate for each nephelometer was 2.6 LPM. The aerosol scattering ($\sigma_{sca, \lambda}$) and backscattering coefficients ($\sigma_{bsca, \lambda}$) were detected in a dry state (RH <35%) and at a controlled RH level of 85 ± 1%, respectively, with the humidification efficiency regulated automatically by a temperature-controlled water bath. More details on the home-built humidified nephelometer system are available in Kuang et al. (2017, 2020) and Xue et al. (2022).

Hence, f(RH) could be calculated as the ratio of the aerosol scattering coefficient at a predefined RH ($\sigma_{sca, RH}$) to the dry ($\sigma_{sca, dry}$) state, i.e., $f(RH) = \sigma_{sca, RH} / \sigma_{sca, dry}$ (Covert et al., 1972). In this study, the f(RH) discussed is mainly targeted for the 525 nm wavelength, unless otherwise specified. More information about the measurement of humidified nephelometer system was illustrated in Sect. S2 of the supplement.

In additional to *f*(RH), aerosol optical parameters, such as scattering Ångström exponent (SAE; Schuster et al., 2006) and hemispheric backscattering fraction (HBF; Collaud Coen et al., 2007), were calculated as below:

$$SAE_{\lambda 1/\lambda 2} = \frac{-\ln(\sigma_{sea, \lambda 1}/\sigma_{sea, \lambda 2})}{\ln(\lambda 1/\lambda 2)}$$
 (1)

$$HBF_{\lambda} = \frac{\sigma_{bsca, \lambda}}{\sigma_{sca, \lambda}}$$
 (2)

where $\sigma_{sca,\ \lambda}$ and $\sigma_{bsca,\ \lambda}$ represent the aerosol scattering and backscattering coefficients at a specific wavelength λ (e.g., $\lambda 1$, $\lambda 2$), respectively.

Both HBF and SAE reflect crucial optical properties of aerosols, e.g., an elevated HBF (or SAE) generally signifies a higher concentration (or a smaller particle size) of fine particles within the aerosol population (Jefferson et al., 2017; Kuang et al., 2017; Luoman et al., 2019). The HBF and SAE discussed in this study are targeted for the dry condition, unless otherwise specified. Based on the measurements with the humidified nephelometer system, the equivalent aerosol liquid water content (ALWC) and the corresponding fraction of ALWC (f_W) can also be obtained (Kuang et al, 2018; see Sect. S2 of the supplement).

The SMPS-measured concurrent particle number size distributions were further utilized to calculate the aerosol effective radius (R_{eff}) and representative parameters for NPF events, e.g., the formation rate (FR) and growth rate (GR) of new particle, condensation sink (CS) and coagulation sink (CoagS) (Dal Maso et al., 2005; Kulmala et al., 2012). More details are provided in the supplement (Sect. S5).

Results of the offline chemical analysis with TSP filter samples are provided in Sect. S3 and Fig. S3. It should be noted that certain secondary organics and crustal elements (e.g., Ca²⁺, Mg²⁺) that could exhibit a broader size distribution may contribute to the observed discrepancy in the total mass concentration between the 24-h TSP samples and daily mean PM_{2.5} (of similar temporal variations; Fig.S3) (Duan et al., 2024; Kim et al., 2020; Xu et al., 2021). Nonetheless, previous studies reported that key components such as SNA (i.e., SO₄²⁻, NO₃⁻, and NH₄⁺) and primary organics of PM_{2.5} (or PM₁₀) were predominantly concentrated within the submicron size range (An et al., 2024; Bae et al., 2019; Chen et al., 2019; Duan et al., 2024; Kim et al., 2020; Xu et al., 2024). While the use of TSP samples contains some uncertainties, the bulk chemical information remains reasonable for characterizing the optical and hygroscopic properties of PM_{2.5}. The descriptions of simultaneous meteorological and air quality data can be found in Sect. S4, and the 48-h/72-h backward trajectory analysis was given in Sect. S5 of the supplement.

2.2.2 Determination of the aerosol direct radiative forcing (ADRF) enhancement factor

Given the high sensitivity of aerosol optical properties (e.g., f(RH)) to the changes in RH under real atmospheric conditions, the influence of RH, or rather the aerosol hygroscopicity, on ADRF can be quantitatively estimated with the radiative transfer model by the following equation (Chylek and Wong, 1995; Kotchenruther et al., 1999; L. Zhang et al., 2015):

217
$$\Delta F_R(RH) = -(S_0/4) \times [T_a^2 \times (1 - A_C)] \times [2 \times (1 - R_s)^2 \times \beta(RH) \times \tau_s - 4 \times R_s \times \tau_a]$$
 (3)

where S_0 is the solar constant, T_a is the atmosphere transmittance, A_C is the fractional cloud amount, R_s is the albedo of the underlying surface, $\beta(RH)$ is the

upscattering fraction at a defined RH, τ_s and τ_a are the optical thicknesses of the aerosol layer due to light scattering and light absorption, respectively, which can be expressed as follows (Kotchenruther et al., 1999):

223
$$\tau_s = M \times \alpha_s \times f(RH), \tau_a = M \times \alpha_a \tag{4}$$

- where M is the column burden of aerosol (unit: gm^{-2}), α_s is the mass scattering efficiency (MSE), and α_a is the mass absorption efficiency (MAE). The direct radiative forcing is usually calculated with the assumption that the absorption enhancement is negligible, in comparison to the aerosol scattering enhancement (Xia et al., 2023).
- Hence, the dependence of ADRF on RH (i.e., $f_{RF}(RH)$) can be estimated by equation (5) (Chylek and Wong, 1995; Kotchenruther et al., 1999; L. Zhang et al., 2015):

232
$$f_{RF}(RH) = \frac{\Delta F_R(RH)}{\Delta F_R(dry)} = \frac{(1 - R_s)^2 \times \beta(RH) \times \alpha_s \times f(RH) - 2 \times R_s \times \alpha_a}{(1 - R_s)^2 \times \beta(dry) \times \alpha_s \times f(dry) - 2 \times R_s \times \alpha_a}$$
(5)

where the constant parameters used were $R_s = 0.15$, $\alpha_a = 0.3 \text{ m}^2 \cdot \text{g}^{-1}$ (Hand and Malm, 2007; Fierz-Schmidhauser et al., 2010). It should be noted that the assumed constant α_a might introduce some uncertainty in the calculated $f_{RF}(RH)$, given the fact that the contribution of absorption by brown carbon was unknown, although the mass fraction of BC in TSP remained almost constant (i.e., $4.6\% \pm 1.1\%$, Fig. S3) during the observation period. The parameter α_s was calculated by dividing $\sigma_{sca, 525}$ in the dry condition by the mass concentration of $PM_{2.5}$ (i.e., $\alpha_s = \sigma_{sca, 525} / PM_{2.5}$). β could be calculated empirically from the measured HBF: $\beta = 0.0817 + 1.8495 \times HBF - 2.9682 \times HBF^2$ (Delene and Ogren, 2002).

3 Results and discussion

3.1 Overview of the aerosol optical hygroscopicity and PNSD measurements

Figure 1 displayed the time series of the measured aerosol scattering coefficients, f(RH), PNSD, and the corresponding meteorological conditions and air pollutants during the study period. A sharp decrease in aerosol scattering coefficients and PM_{2.5},

accompanied with the continuous excellent visibility over 20 km was observed after August 6, indicating a markedly cleaner environment during P2 in comparison to P1 in summer 2022 of Chongqing. This could be largely attributed to the reduction in anthropogenic emissions (e.g., NO₂, CO, except SO₂) from limited outdoor activities influenced by the heatwaves in P2, as well as partly suspended industries and transportation to alleviate the power shortage issue (Chen et al., 2024). Notably, the increased wind speed and enhanced mixing layer height (MLH) also enabled a more favorable atmospheric diffusion condition in P2, facilitating the dilution of surface air pollutants (Zhang et al., 2008). However, a higher mass concentration of SO₂ was observed in the P2 period, likely due to a surge in electricity demand and resulted higher emissions from power plants operating almost at full capacity during the heatwave (Su, 2021; Teng et al., 2022). Moreover, significant discrepancies in the aerosol optical and hygroscopic properties were observed under different synoptic conditions (Table S2). Both HBF and SAE were higher during the P2 period, aligning with the smaller R_{eff} (Table S2). The f(RH) was found to be relatively higher (p < 0.05) in heatwave days, with the mean values of 1.61 ± 0.12 and 1.71 ± 0.15 during the P1 and P2 periods, respectively. Differently, ALWC was more abundant during the normally hot P1 period than the heatwave-dominated P2 period. This is likely due to that the derivation algorithm of ALWC utilized in this study (Kuang et al., 2018) was partly dependent on (e.g., positively correlated) the dry aerosol scattering coefficient, or rather the aerosol volume concentration in the dry condition (refer to Sect. S3 and Fig. S11 of the supplement). The mean $\sigma_{sca. 525}$ for P2 was about 46.8% of that for the P1 period, and the corresponding mean level of ALWC was approximately 55.8% of that for P1. This partly agrees with the stronger aerosol optical hygroscopicity with a marginally higher f_W during the P2 period, highlighting a complex interaction between the optical enhancement and aerosol physicochemical properties.

247

248

249

250

251

252

253

254

255

256

257

258

259

260

261

262

263

264

265

266

267

268

269

270

271

272

273

274

275

276

The particle number size distribution data suggested that NPF events appeared in about half the number of observation days (Fig. 1i), with an overall occurrence frequency of 52.4% (Fig. S4a). This suggests the rather frequent summer NPF events in Chongqing, notably higher than those observed in other regions of the world, e.g.,

Beijing (16.7%, Deng et al., 2020; ~20%, Wang et al., 2013), Dongguan (4%, Tao et al., 2023), Hyytiälä (<40%, Dada et al., 2017) and LiLLE (<20%, Crumeyrolle et al., 2023). Moreover, the frequent NPF events during heatwaves formed substantially ultrafine particles that are of less contribution to aerosol optical properties in comparison to large particles (Fig. S13), partially explaining the significantly lower levels of total scattering coefficients observed during the P2 period. It should be noted that the hourly $\sigma_{sca, 525}$ values during the P2 period were exclusively below 100 Mm⁻¹ (approximately the last 10^{th} percentile of $\sigma_{sca, 525}$ data, regarded as the threshold value of relatively polluted cases; Fig. S2c), suggesting a much cleaner environment compared to the relatively polluted P1 period. Correspondingly, NPF events occurring during the relatively polluted P1 period (as detailed in section 3.2) were defined as NPF_{polluted}, while cases during the cleaner and heatwave-dominated P2 period were classified as NPF_{clean, HW}.

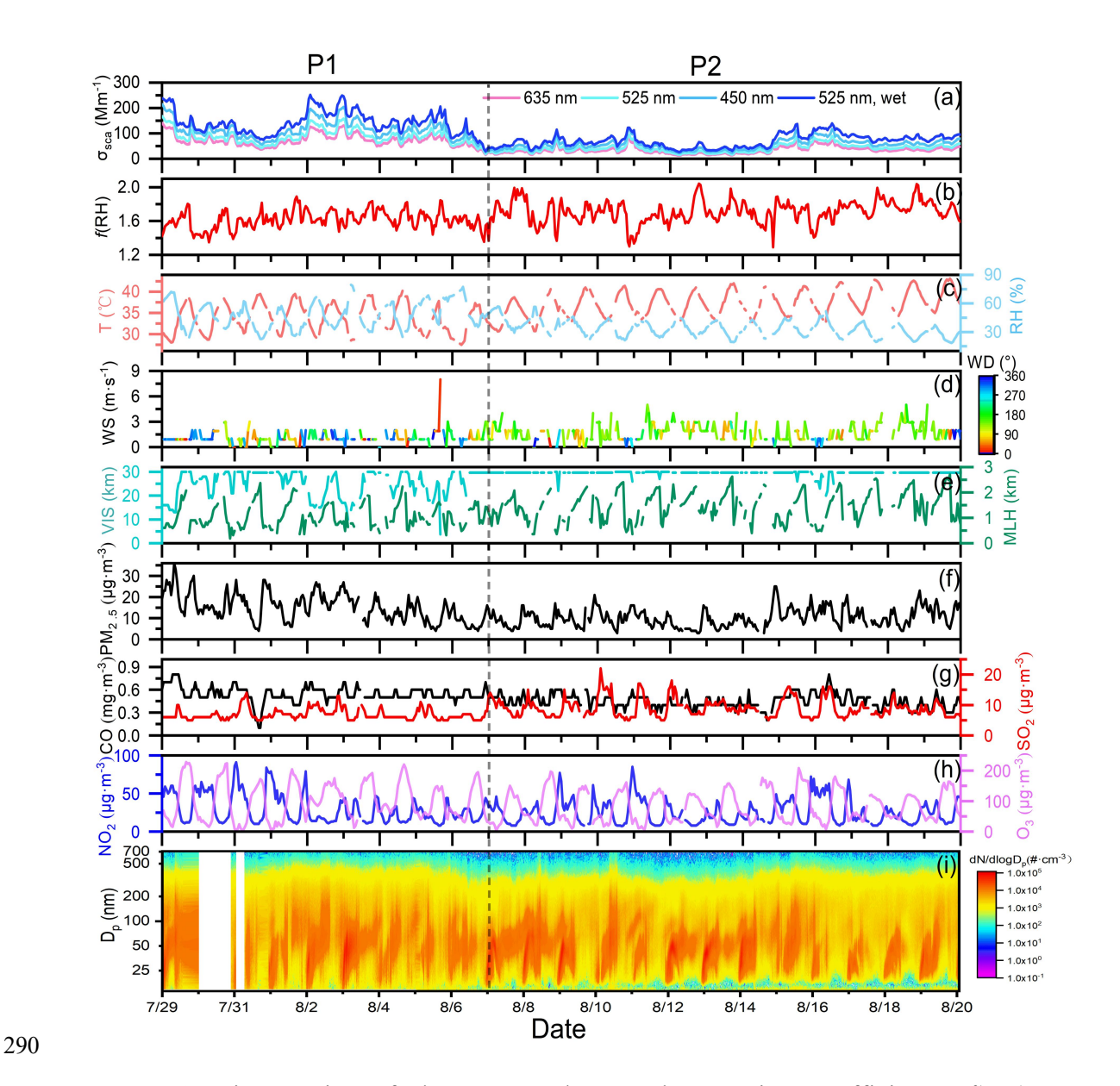


Figure 1. Time series of the measured aerosol scattering coefficients, f(RH), meteorological conditions, air pollutants, and particle number size distribution during the study period.

3.2 Characteristics of NPF events in different periods

Aside from gaseous precursors (e.g., SO₂, volatile organic compounds), meteorological conditions also play a key role in the occurrence of NPF events. In brief, NPF events are more likely to appear under sunny and clean conditions (Bousiotis et al., 2021; Crumeyrolle et al., 2023; Deng et al., 2021; Wang et al., 2017). The backward trajectory analysis revealed that the southerly breeze was predominant during the study period (Fig. S4b). Although the surface wind vector slightly varied

between the P1 and P2 periods, this consistency in air mass origins suggests that some other factors (e.g., changes in environmental conditions and emissions of gaseous precursors under heatwaves) could have played a crucial role in modulating NPF events. To further explore the characteristics of NPF events in different periods, the time-averaged diurnal variations of meteorological parameters and air pollutant concentrations during both NPF events and non-event days are presented in Fig. 2.

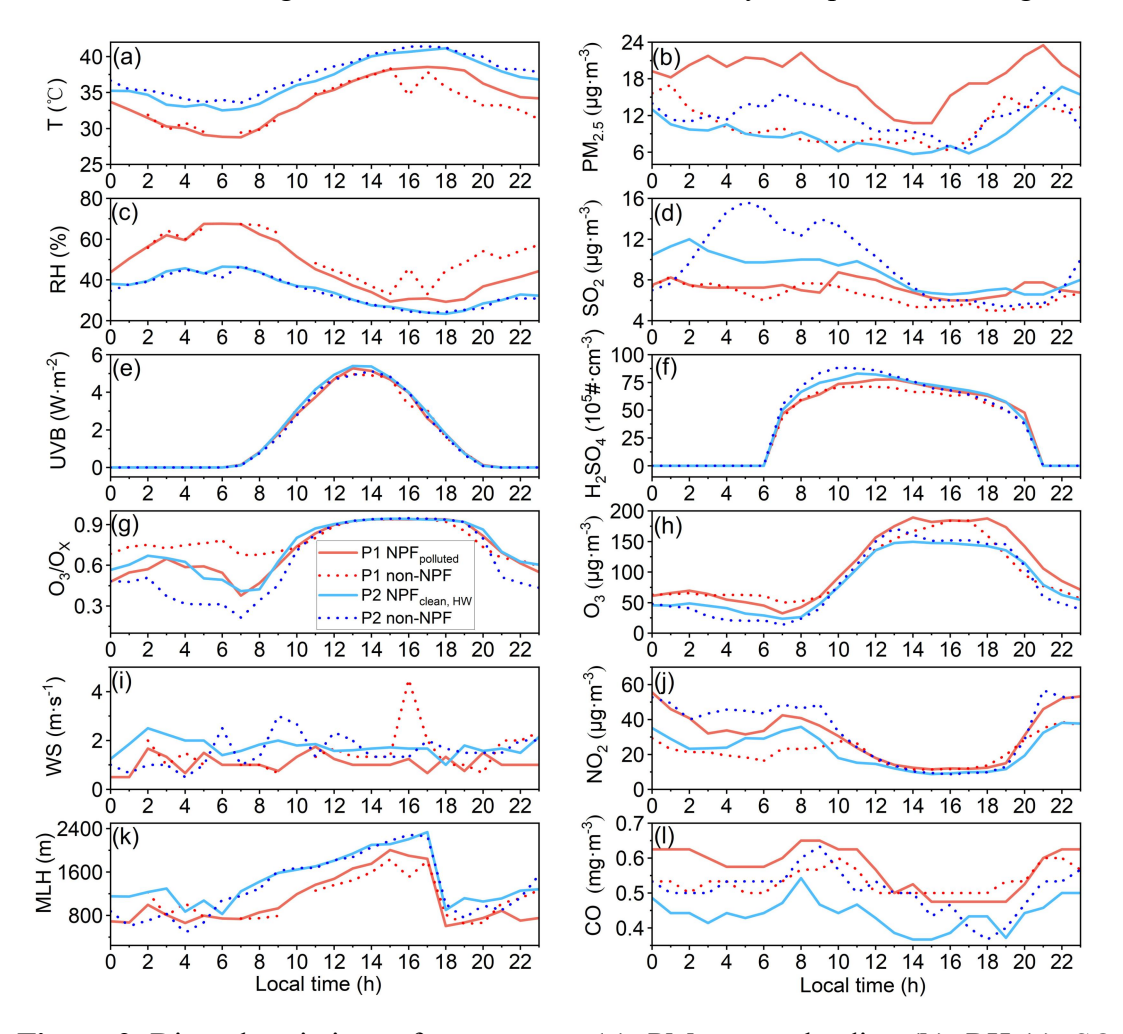


Figure 2. Diurnal variations of temperature (a), PM_{2.5} mass loading (b), RH (c), SO₂ (d), UVB (e), H₂SO₄ (f), O₃/O_X (g), O₃ (h), WS (i), NO₂ (j), MLH (k) and CO (l) during P1 (red) and P2 (blue) NPF days (solid line), as well as the corresponding non-event days (dash line).

As stated in Sect.3.1, NPF events during the P1 period tended to occur in relatively polluted environments compared to that of P2 NPF_{clean, HW} events, as evidenced by the frequent occurrence of $\sigma_{sca, 525} > 100$ Mm⁻¹, increased air pollutant

concentrations and lower visibility levels during P1 (Table S2, Fig. 1). Additionally, the mean CS of the NPF_{polluted} events was above 0.015 s⁻¹ (Table S2), which could be considered as the "polluted" NPF cases (Shang et al., 2023). On P2 NPF_{clean, HW} days, the overall mean $\sigma_{sca, 525}$ was 33.2 \pm 11.7 Mm⁻¹, decreased by 68.0% (39.3%) in comparison to that for P1 NPF_{polluted} days (P2 non-event days). In addition, the mean PM_{2.5} concentration was even lower than 10.0 μ g·m⁻³, and the corresponding visibility level was almost maintained at 30 km (Fig. 1e). All the above implies that the P2 NPF_{clean, HW} events were generally accompanied with a much cleaner environment. It is notable that the increase in SO₂ concentration after 9:00 LT (Fig. 2d), along with the significant decrease in PM_{2.5} mass loadings after 8:00 LT during P1 NPF_{polluted} events (Fig. 2b), likely favored the occurrence of NPF events. The higher gas-phase sulfuric acid (i.e., H₂SO₄, as estimated with the UVB and SO₂ concentration, Lu et al., 2019, Sect. S4) on the same NPF days (Fig. 2f), further suggesting that sulfuric acid concentration was a critical factor for the occurrence of P1 NPF_{polluted} events.

The diurnal evolutions of meteorological conditions (e.g., T, RH, MLH) for NPF events were distinct between P1 and P2 periods, although relatively insignificant differences were observed for both NPF days and non-event days within a same period (Fig. 2). This likely suggests that meteorological factors might not be the predominant determining factor of NPF occurrence during the heatwaves of 2022 summer in urban Chongqing, while NPF could be accompanied with quite different meteorological conditions depending on gaseous precursors and preexisting condensation sinks. For instance, the NPF_{clean, HW} events were typically of clean-type NPF, characterized with lower background aerosol loading, higher temperature and favorable atmospheric dispersion capacity with the higher MLH. However, it is reported that excessive heat can increase the evaporation rate of critical acid-base clusters during the nucleation process and reduce the stability of initial molecular clusters (Bousiotis et al., 2021; Kurtén et al., 2007; Zhang et al., 2012), in line with a recent study that NPF events were weaker during heatwaves in Siberian boreal forest due to the unstable clusters (Garmash et al., 2024). On the other hand, the emission rate of biogenic VOCs (BVOCs, e.g., isoprene, monoterpene) from nearby plants and trees would decrease when temperature exceeded around 40 °C (Guenther et al., 1991; Pierce and Waldruff, 1991), despite that BVOCs plays a key role in the nucleation mechanism of NPF (Wang et al., 2017; Zhang et al., 2004). Hence, the even higher temperature (e.g., T >40 °C) likely suppressed the nucleation processes and the subsequent growth of nucleation mode particles on P2 non-event days (Fig. S6b2), in spite of higher concentrations of SO₂ and H₂SO₄.

345

346

347

348

349

350

351

352

353

354

355

356

357

358

359

360

361

362

363

364

365

366

367

368

369

370

371

372

373

374

To further investigate the effect of heatwave on NPF events, the diurnal variations of PNSD, Reff and particle mode diameter (Dmode) were shown in Fig. S6. Aerosol number and volume concentrations, as well as Reff, for different modes were illustrated in Figs. S7-8, and the relationship between temperature and the duration of NPF events was displayed in Fig. S9. Distinct particle size distributions were observed for different NPF event days. While the number concentrations of Aitken mode particles (N_{Ait.}) were comparable during NPF days of both periods, the corresponding number concentration of nucleation mode (N_{Nuc.}) was significantly higher on P1 NPF_{polluted} days (1880.8 \pm 2261.5 cm⁻³) than that for P2 NPF cases $(1132.0 \pm 1333.5 \text{ cm}^{-3})$ (Fig. 1i, Fig. S7). Different from that of the P1 NPF_{polluted} cases, the P2 NPF_{clean, HW} event did not start from the minimum size, and the reduced N_{Nuc.} during P2 period was likely attributed to the influence of transport on the local nucleation and growth process (Fig. S4; Cai et al., 2023; Lee et al., 2019). Namely, some nucleation mode particles transported from upwind regions or from the mixing layer downwards had undergone atmospheric aging thereby a certain degree of growth upon arrival (Cai et al., 2023; Lai et al., 2022; Platis et al., 2016), resulting in relatively lower concentrations of smaller-sized particles than the case of locally formed. However, the local formation of sub-25 nm particles and the continuous growth process were still distinctly observed under heatwaves (Fig. 1i, Figs. S6, S15). The NPF events under heatwaves usually initiated earlier (Fig. S9), with the N_{Nuc.} in P2 NPF_{clean, HW} cases peaked about an hour earlier in comparison to NPF_{polluted} days (Fig. S8a). The D_{mode} on P2 NPF_{clean, HW} days also reached its minimum earlier than that on P1 NPF_{polluted} days (Fig. S6). Since the sunrise and sunset time did not significantly vary within the study period (i.e., less than a half hour discrepancy),

heatwaves likely provided more favorable conditions (e.g., enhanced volatile gaseous emissions, low RH; Bousiotis et al., 2021; Hamed et al., 2007; Wang et al., 2024) for the occurrence of NPF events in urban Chongqing. This is supported by the earlier start time of NPF_{clean}, HW corresponding to higher temperature ranges (Fig. S9). Furthermore, the end time of subsequent particle growth during P2 period was even later (i.e., ~ 21:00 LT) than that of P1 cases (Fig. S9). Given that the growth rates of new particles were generally lower during P2 NPF_{clean, HW} events (Table S2), these explosively formed new particles could persist longer in the warmer atmosphere and probably undergo aging processes with a relatively higher oxidation degree. This is supported by the commonly higher ratios of secondary organic carbon (SOC) to organic carbon (OC) (i.e., SOC/OC >0.5) during the NPF_{clean, HW} days (Fig. S3b). In addition, aerosol Reff was significantly smaller on the NPFclean, HW days under heatwave conditions. The Reff and Dmode nearly kept at a same level below/approaching 50 nm during the subsequent growth on the P2 NPF_{clean, HW} days, while the R_{eff} was generally above 50 nm and larger than D_{mode} for both P1 NPF_{polluted} cases and non-event days (Fig. S6). The diurnal patterns of aerosol volume concentrations for different size modes were similar to that of aerosol number concentrations during NPF events (Fig. S8b1-b3). However, both the Reff of Aitken mode particles (R_{Ait.}) and accumulation mode particles (R_{Acc.}) were smaller during P2 NPF_{clean, HW} events than that of P1 NPF_{polluted} events (Fig. S8c2-c3), which may further influence size-dependent aerosol optical and hygroscopic properties (e.g., $\sigma_{sea.}$ 525, HBF, SAE, f(RH)). The decrease in RAit. and RAcc. during heatwaves could be attributed to three factors: (1) evaporation of the outer layer of particles and unstable clusters due to heatwaves (Bousiotis et al., 2021; Cusack et al., 2013; Deng et al., 2020; Garmash et al., 2024; Li et al., 2019); (2) lower FR and GR of particles under the cleaner environment (Table S2); (3) reduced emissions of larger primary particles during the P2 period.

375

376

377

378

379

380

381

382

383

384

385

386

387

388

389

390

391

392

393

394

395

396

397

398

399

400

3.3 Characteristics of the aerosol optical and hygroscopic properties on different types of NPF days

Diurnal variations of the aerosol optical and hygroscopic parameters during different NPF days were shown in Fig. 3, and the corresponding results for non-event days can refer to Fig. S10. Generally, $\sigma_{sca, 525}$ possessed a similar bimodal diurnal pattern to that of the accumulation mode aerosol volume concentration ($V_{Acc.}$) (Fig. S8b3), as supported by the positive correlation between $\sigma_{sca, 525}$ and SMPS-measured aerosol volume concentration (Fig. S12). This is also consistent with the Mie theory, with a stronger increase in the scattering efficiency for accumulation mode particles (Titos et al., 2021). The diurnal pattern of $\sigma_{sca, 525}$ also varied distinctly between different NPF days. Specifically, a minor peak of $\sigma_{sca, 525}$ around 12:00 LT (Fig. 3a) was influenced by the newly formed particles during P2 NPF_{clean, HW} events, which contributed more significantly to the aerosol number and volume concentrations within 100 nm size ranges in markedly clean environments (Fig. S5c1, c2). Instead of a noontime peak, $\sigma_{sca, 525}$ was observed with an early peak around the morning rush hours and a maximum value similarly occurred at the nighttime on P1 NPF_{polluted} days.

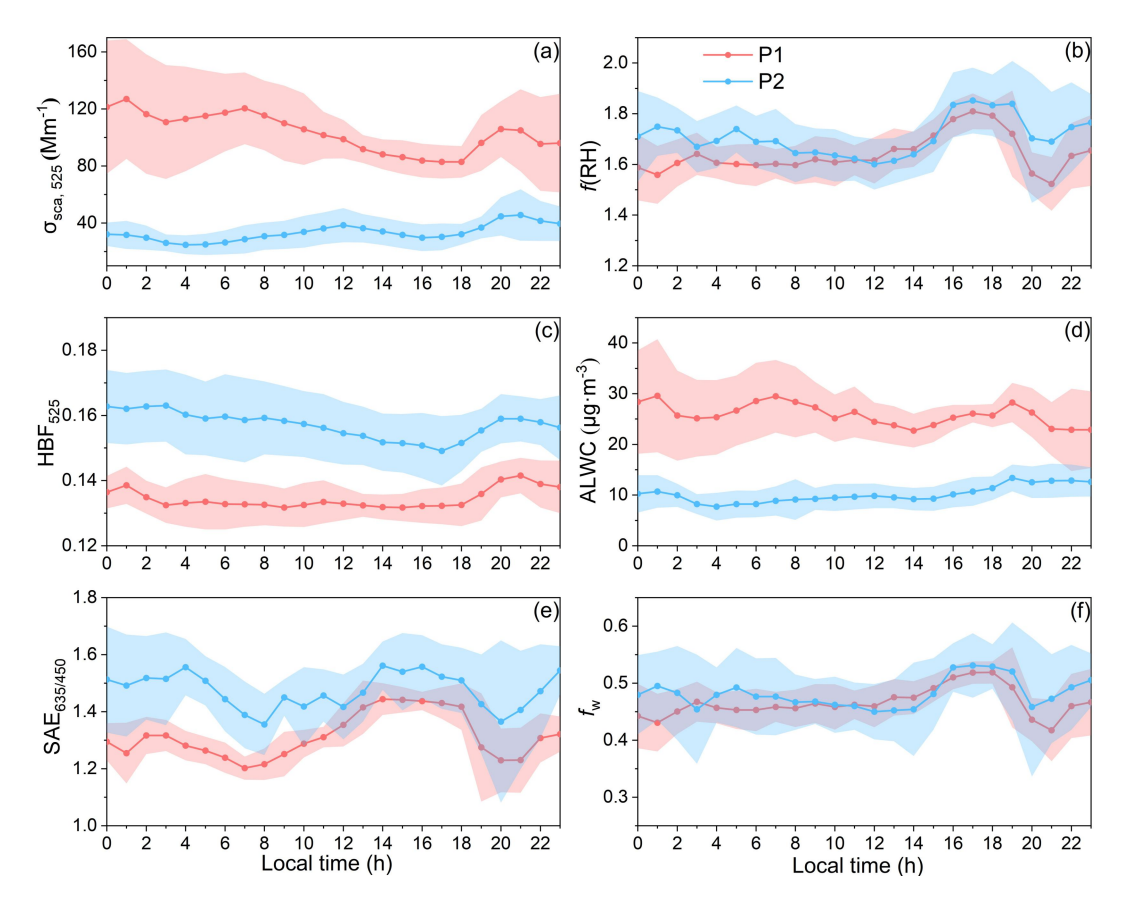


Figure 3. Diurnal variations of σ_{sca} , 525 (a), f(RH) (b), HBF525 (c), ALWC (d),

SAE_{635/450} (e) and f_W (f) on NPF days during P1 (red line) and P2 (blue line) periods.

The shaded areas stand for the corresponding $\pm 1\sigma$ standard deviations.

421

422

423

424

425

426

427

428

429

430

431

432

433

434

435

436

437

438

439

440

441

442

443

444

445

446

447

Both HBF and SAE on P2 NPF_{clean, HW} days were significantly higher than that of P1 NPF_{polluted} cases (Fig. 3c, e), largely due to the smaller R_{eff} observed during heatwave-dominated period (Table S2). Moreover, the correlation between HBF (or SAE) and particle size in each mode was weaker on NPF days than on non-event days, especially for NPF_{clean, HW} days (Fig. S14). A strongest negative correlation was found between HBF and Reff of the accumulation mode in comparison to other modes, highlighting that HBF is more sensitive to the size distribution of accumulation mode particles (Collaud Coen et al., 2007). Given that NPF would largely enhance the abundance of both nucleation and Aitken mode aerosols (Fig. S7), no significant variation in HBF was observed during the daytime due to the weakened correlation between HBF and RAcc. of NPF events. SAE is commonly used as an indicator of particle size distribution, almost decreasing monotonously with the increase of aerosol size within 1 µm (Kuang et al., 2017, 2018; Luoma et al., 2019). Accordingly, SAE decreased over the morning and evening rush hours when coarse particles (e.g., aged particles, road dust, automobile exhaust) generated during anthropogenic activities, accompanied with an increase in CO that is taken as the proxy for primary emissions (Fig. 21) (Yarragunta et al., 2020). On the contrary, the abundant ultrafine particles formed during NPF events led to a continuous increase in SAE during the day.

f(RH) exhibited a similar diurnal pattern on the P1 and P2 NPF days (Fig. 3b). During the daytime, f(RH) remained relatively stable and gradually increased until peaking around 16:00-18:00 LT, with a generally higher f(RH) particularly after 15:00 LT during P2 NPF_{clean, HW} days than that of P1 cases. The insignificant fluctuation of relatively lower f(RH) levels before the noon could be attributed to the continuous development of the mixing layer (Fig. 2k), leading to an efficient mixing of particles in the nocturnal residual layer with anthropogenic emissions near the ground. Additionally, photochemical reactions in the afternoon facilitated the formation of

more hygroscopic secondary aerosols with a higher oxidation level (Liu et al., 2014; R. Zhang et al., 2015). The diurnal patterns of O₃ and the O₃/O_X ratio (i.e., an indicator of atmospheric oxidation capacity, where $O_X = O_3 + NO_2$, Tian et al., 2021) also showed similar trends (Fig. 2g, 2h). The presence of black carbon (BC) mixed with organic compounds (e.g., from traffic emissions and residential cooking activities) explained the rapid decrease in f(RH) during the evening rush hours (Liu et al., 2011). Furthermore, the daily mean f(RH) for NPF days was higher than that of non-event days (Table S2), particularly after the ending of NPF events around 12:00 LT. Given that newly formed particles were too small to significantly impact the total light scattering (Fig. S11a), this indicates that the atmospheric conditions conducive to the occurrence of NPF may promote further growth (e.g., via intensified/prolonged photooxidation or atmospheric aging processes) of pre-existing particles and newly formed ones, leading topartly contributing to enhanced aerosol optical hygroscopicity as clued from the concurrent variations of ALWC and $f_{\rm W}$ in urban Chongqing during hot summer (Asmi et al., 2010; Wang et al., 2019; Wu et al., 2016). The diurnal pattern of ALWC closely mirrored the variation in $\sigma_{sca, 525}$, while f_W followed the similar evolution of f(RH). This suggests that ALWC was more sensitive to changes in the aerosol volume concentration, as determined by the corresponding retrieval algorithm (Kuang et al., 2018). The $f_{\rm W}$ levels were slightly higher during NPF days in comparison to that of non-event days (Table S2). This difference was more pronounced in the afternoon of NPF days (e.g., even exceeded 50%; Fig. 3f), verified the enhancement of aerosol hygroscopicity during the subsequent growth and atmospheric aging of both pre-existing and newly formed particles.

448

449

450

451

452

453

454

455

456

457

458

459

460

461

462

463

464

465

466

467

468

469

470

471

472

473

474

475

476

3.4 Heatwave-induced divergent changes in aerosol optical hygroscopicity

To further explore the impacts of heatwaves on *f*(RH) during diverse NPF events, data mainly within the time window of 08:00-22:00 LT (i.e., typically covered the complete process of NPF and subsequent growth, while excluded higher RH conditions at night) were utilized for the following discussion.

Although ultrafine particles exhibited higher number concentrations during the

study period, accumulation mode particles dominated the aerosol volume concentration and contributed predominantly to the total light scattering (Figs. S7, S13). A positive correlation between f(RH), R_{eff} and the volume fraction of accumulation mode particles (VF_{Acc.}) was found on non-event days (Fig. 4c-d), when the aerosol size distribution was undisturbed by newly formed ultrafine particles and the corresponding VF_{Acc.} maintained around a high level of 0.95 (Fig. 4a-b). The notably positive correlation between f(RH) and R_{eff} could be linked to the secondary formation of hygroscopic particles within the accumulation mode, primarily via photochemical reactions and further intensified by heatwaves during the non-event day particularly of the P2 period (Gu et al., 2023; Liu et al., 2014; R. Zhang et al., 2015; Zhang et al., 2024). Consequently, f(RH) at a specific R_{eff} was generally higher during the P2 period in comparison to that of P1 (Fig. 4c-d), also with high f(RH) levels observed for smaller size cases of R_{eff} <110 nm under some extremely high temperature conditions (T >40 °C, as highlighted by the red dashed circle in Fig. 4d). The higher SOC/OC on P2 non-event days further demonstrated the stronger secondary aerosol formation in comparison to P1 non-event days (Fig. S3b).

477

478

479

480

481

482

483

484

485

486

487

488

489

490

491

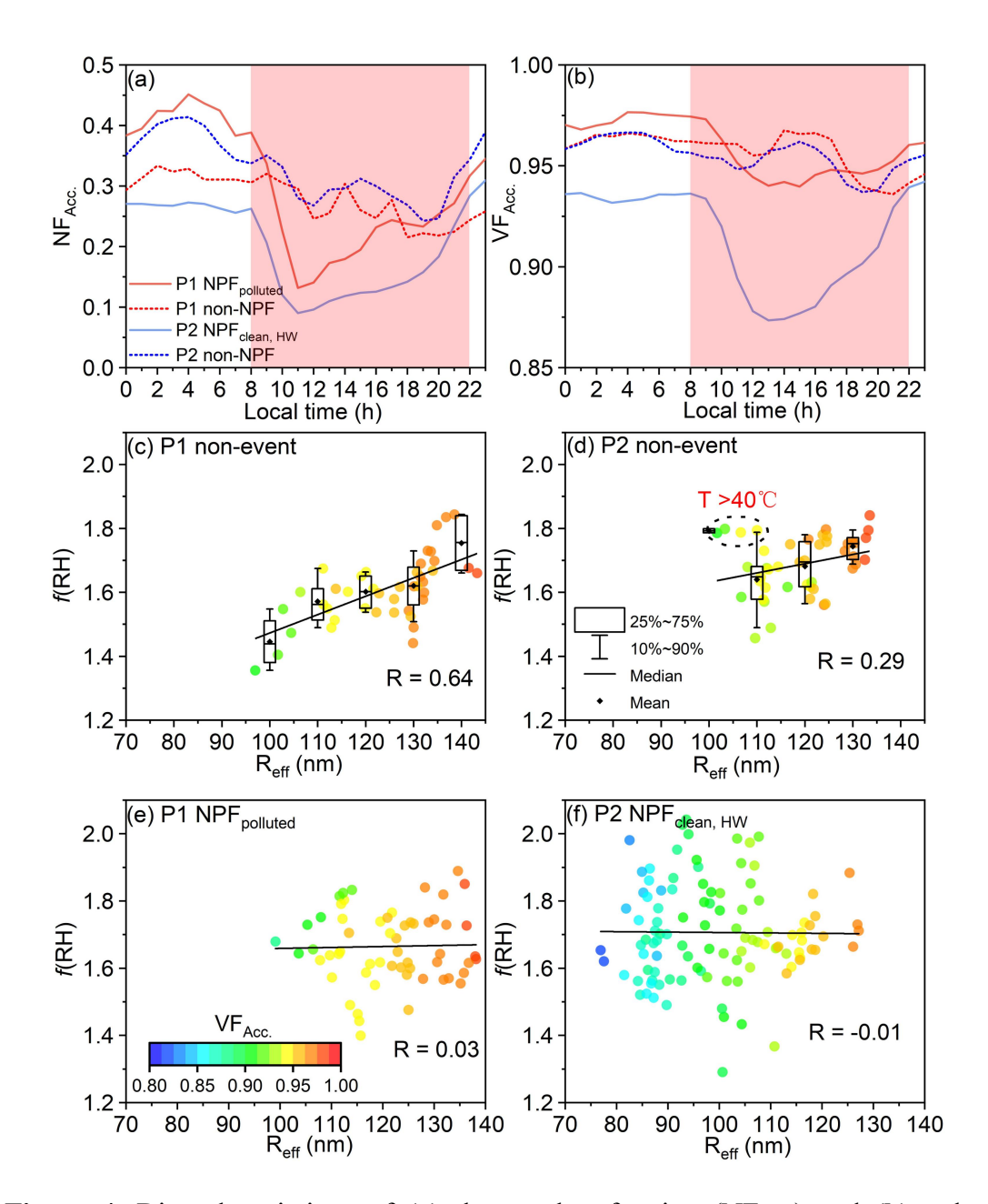


Figure 4. Diurnal variations of **(a)** the number fraction (NF_{Acc.}) and **(b)** volume fraction of accumulation mode particles (VF_{Acc.}) on P1 (red) and P2 (blue) NPF days (solid line), as well as non-event days (dash line). The time window of 08:00-22:00 LT was shaded in red. The relationship of *f*(RH) with R_{eff} and VF_{Acc.} (as indicated by the colored dots) on P1 **(c)** and P2 non-event days **(d)**, as well as on P1 **(e)** and P2 **(f)** NPF days during the 08:00-22:00 LT time window.

Nevertheless, f(RH) was almost independent of the two parameters (i.e., R_{eff} and VF_{Acc.}) for NPF events (Fig. 4e-f). This is mainly due to the explosive formation of ultrafine particles and subsequent growth on NPF days, significantly altering

aerosol size distributions and inducing large fluctuations in the NF_{Acc.} and VF_{Acc.} in comparison to that on non-event days, especially during the P2 period (as shaded in Fig. 4a-b). Therefore, characterizing f(RH) with the corresponding R_{eff} of aerosol populations was no longer applicable. Alternatively, SAE was commonly used to estimate or parameterize f(RH) (Titos et al., 2014; Xia et al., 2023; Xue et al., 2022), in line with the similar diurnal patterns of f(RH) and SAE observed in this study. Figure 5 demonstrated a significantly positive correlation between f(RH) and SAE during NPF days in comparison to non-event days, with a similar slope of approximately 0.65 suggesting the consistent variation of f(RH) with SAE across both periods. As larger particles contributed higher to the aerosol volume concentrations (Fig. S5), the decrease of SAE also corresponded to an increase in $\sigma_{sca, 525}$ (Fig. 5a3, b3). Given that larger $\sigma_{sca, 525}$ values typically indicate the condition of a higher aerosol loading, f(RH) increased with SAE whereas decreased with $\sigma_{sca, 525}$, or rather the pollution level, during NPF days. The cleaner environment of P2 period may further favor the occurrence of NPF events. Both f(RH) and SAE exhibited a higher level on P2 NPF_{clean, HW} days (as shown by the dash lines in Fig. 5), likelyprobably attributed to the following two aspects. One is related to the smaller aerosol Reff (with a larger SAE) due to the lower FR and GR, likely influenced by the evaporation of newly-formed unstable clusters and particle coatings under heatwaves (Bousiotis et al., 2021; Cusack et al., 2013; Deng et al., 2020) during the subsequent growth of aerosols. Secondly, the higher temperature was normally associated with stronger photochemical oxidation, which could intensify the formation of secondary aerosol components with a higher hygroscopicity (Asmi et al., 2010; Gu et al., 2023; Liu et al., 2014; Wu et al., 2016; R. Zhang et al., 2015; Zhang et al., 2024). This is further supported by the slightly higher levels of UVB (P1: $2.6 \pm 1.9 \text{ W} \cdot \text{m}^{-2}$ versus P2: $2.7 \pm 1.9 \text{ W} \cdot \text{m}^{-2}$ 2.0 W·m⁻²) and O_3/O_X (P1: 0.81 ± 0.17 versus P2: 0.82 ± 0.17) during P2 heatwave days, also in line with a recent study which demonstrated that heatwaves affected secondary organic aerosols (SOA) formation and aging by accelerating photooxidation in Beijing (Zhang et al., 2024).

503

504

505

506

507

508

509

510

511

512

513

514

515

516

517

518

519

520

521

522

523

524

525

526

527

528

529

530

531

532

It is worth noting that f(RH) did not show a consistently higher level after the

NPF_{clean, HW} occurrence during P2 period, and it was slightly higher within the first few hours of NPF occurrence (i.e., ~ 12:00 -15:00 LT) on P1 NPF_{polluted} days (Fig. 3b). In fact, aerosol optical hygroscopicity not fully corresponds to the bulk hygroscopicity primarily determined by aerosol chemical components, and the variability in aerosol optical features also plays a key role in f(RH). Hence, the size-dependency of aerosol optical properties should be considered. The size-resolved $\sigma_{sca, 525}$ distribution and size-resolved cumulative frequency distribution (CFD) of $\sigma_{sca, 525}$ over different NPF days were calculated using the Mie theory, with good agreements between the theoretically calculated and measured $\sigma_{sca, 525}$ values (R² = 0.99). As shown in Fig. S11a and Fig. S13, new particles must grow into the accumulation mode size at least before they can exert a significant influence on the total scattering coefficient. The critical sizes corresponding to the cumulative frequency of 50% in $\sigma_{sca, 525}$ were 358.7 nm and 333.8 nm on P1 and P2 NPF days, respectively. This indicates that relatively smaller particles including the newly formed and grown ones mixed with pre-existing and aged particles contributed a slightly higher portion to $\sigma_{sca, 525}$ on P2 NPF_{clean, HW} days, while the $\sigma_{sca, 525}$ was mainly contributed by larger ones on P1 NPF_{polluted} days. Nevertheless, the Mie theory suggests that these smaller particles generally have a weaker enhancement in total scattering after hygroscopic growth, in comparison to larger size particles (Collaud Coen et al., 2007, Fig. S11a). Consequently, the changes in aerosol optical and hygroscopic properties necessitate consideration of both aerosol optical and chemical characteristics during different NPF events. Newly formed ultrafine particles contributed minor to aerosol optical properties, resulting in a lower f(RH) during the initial hours of P2 NPF_{clean, HW} events compared to that of P1 NPF_{polluted} events (Fig. 3b), as evidenced by a smaller R_{eff} for P2 NPF_{clean, HW} events (Fig. S6). In contrast, the growth of pre-existing and newly formed particles into larger sizes would subsequently affect bulk aerosol optical properties, which was evidenced by the enhancement in aerosol extinction coefficient observed after NPF occurrence in a recent study (Sun et al., 2024). Specifically, particles could undergo a longer and more intensified photochemical aging process during NPF_{clean, HW} eventdays as influenced by persistent heatwaves, which facilitated the secondary

533

534

535

536

537

538

539

540

541

542

543

544

545

546

547

548

549

550

551

552

553

554

555

556

557

558

559

560

561

formation of hygroscopic aerosols and resulted injointly contributed to a higher f(RH) after 15:00 LT (Fig. 3b).

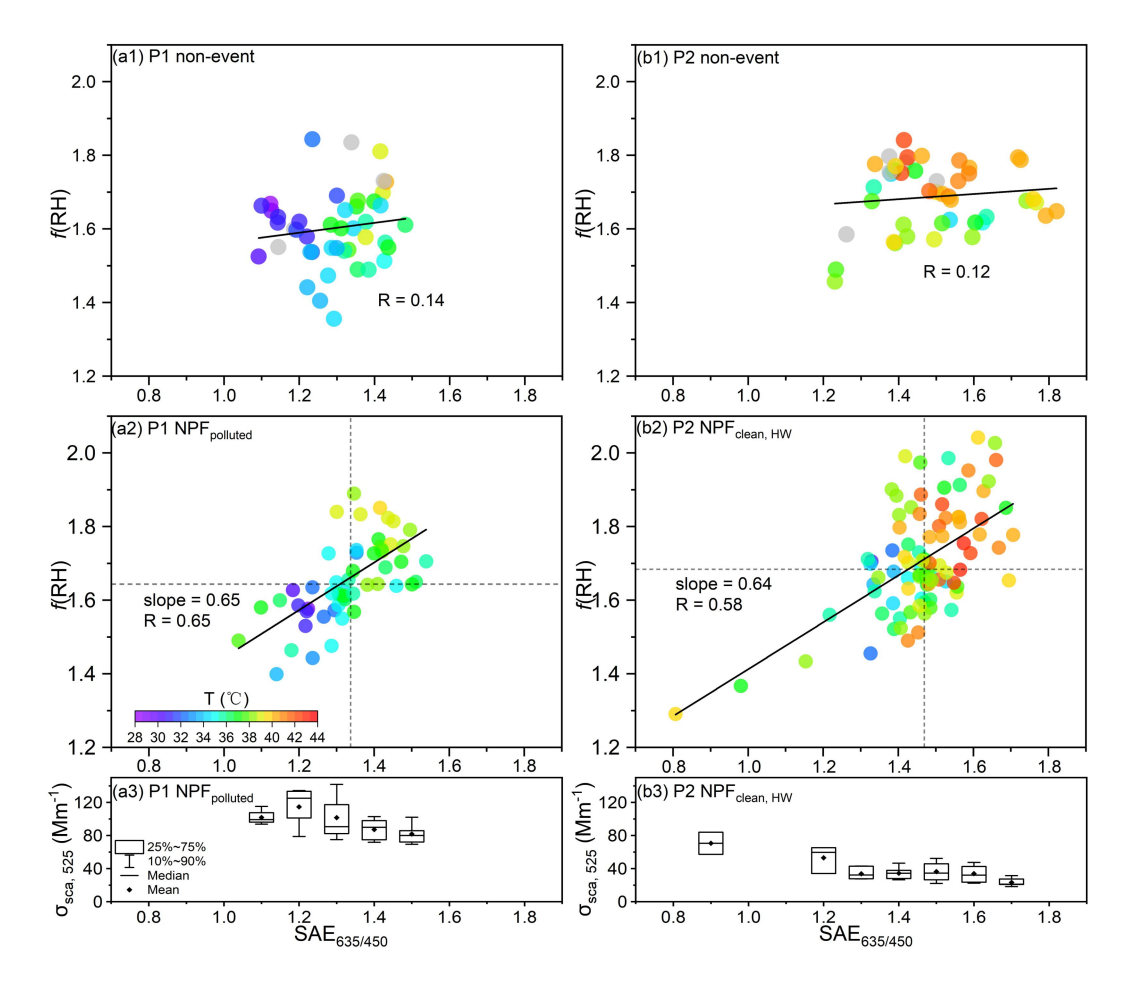


Figure 5. The relationship between f(RH) and $SAE_{635/450}$, as well as temperature (as indicated by the color of dots, missing values are represented in gray), on P1 non-event days (a1), NPF_{polluted} days (a2) during the 08:00-22:00 LT time window. The vertical (horizontal) dash line represents the median value of $SAE_{635/450}$ (f(RH)). (a3) The corresponding $\sigma_{sca, 525}$ under different $SAE_{635/450}$ levels on P1 NPF_{polluted} days. (b1-b3) The same but for P2 period.

3.5 f(RH)-induced changes in aerosol direct radiative forcing

The changes in f(RH) have significant implications for aerosol direct radiative forcing. Despite considerably lower $\sigma_{sca, 525}$ results during heatwaves, the corresponding mean $f_{RF}(RH)$ levels particularly for P2 NPF_{clean, HW} days were higher than that of the P1 cases (Fig. 6a). A robust positive correlation ($R^2 = 0.68$) was observed between f(RH) and aerosol radiative forcing enhancement factor, $f_{RF}(RH)$

(Fig. 6b). This is likely attributed to the enhanced $f_{RF}(RH)$ with the larger forward scattering ratio β , or rather higher HBF for smaller particle sizes, as supported by a generally negative correlation between $f_{RF}(RH)$ and R_{eff} . Specifically, the highest $f_{RF}(RH)$ value of 2.21 \pm 0.23 was observed on P2 NPF_{clean, HW} days, characterized with the highest $f_{RF}(RH)$ and smallest R_{eff} (i.e., highest HBF) of the entire study period.

578

579

580

581

582

583

584

585

586

587

588

589

590

591

592

593

594

595

596

597

598

599

600

601

602

603

604

605

606

607

The definition of $f_{RF}(RH)$ in Eq.(5) implies the dependences of $f_{RF}(RH)$ on both f(RH) and HBF-derived $\beta(RH)$ and $\beta(dry)$, or rather the ratio of HBF_{525. RH}/HBF₅₂₅. The mean HBF_{525, RH} was generally larger than HBF₅₂₅ in this study, specifically with the HBF_{525, RH}/HBF₅₂₅ ratios centered around 1.8 and even approached 2.5 on P2 NPF_{clean, HW} days (Fig. 6c, Table S2). This could be different from the classical Mie theory with the spherical-particle premise, i.e., the observed light backscattering was enhanced after hydration likely resulted from the evolution in particle morphology that significantly influences their optical properties (Mishchenko 2009). Additionally, the predominant organic components when heterogeneously mixed with diverse chemical compositions (e.g., inorganics and black carbon) likely introduced the heterogeneity in aerosol hygroscopicity (Yuan and Zhao, 2023), which may alter particle morphology thereby optical properties upon water uptake (Giordano et al., 2015; Tan et al., 2020; Tritscher et al., 2011). The efficient evaporation of organic coatings under extremely hot conditions could also contribute to the change in particle morphology (e.g., non-spherical inregular shapes) upon humidification, as evidenced by a recent study that high temperature conditions could accelerate the evaporation rate of SOA (Li et al., 2019). Given that the backward scattering intensity of non-spherical particles is suggested to be much larger than its spherical counterparts at scattering angles between 90° and 150° (Mishchenko 2009; Yang et al., 2007) and that the HBF-derived asymmetry parameter (g) normally correlates positively with the aerosol forward scattering (Andrews et al., 2006; Marshall et al., 1995), the generally smaller g_{RH} results (in comparison to g) confirmed the decrease (increase) in the forward (backward) light scattering after water uptake (Fig. S11c), likely implying the change in the morphological structure of particles. This is particularly evident for P2 NPF_{clean, HW} days, with a much lower level of g_{RH} was observed (Fig. S11c). Another

possible reason is the distinct size dependences of both light scattering and backscattering efficiencies (Fig. S11a), with much more significant enhancements in the backscattering efficiency thereby HBF specifically of accumulation mode particles after hygroscopic growth (Fig. S11b). As reflected by the Mie model, although the abundant newly formed particles were generally optically-insensitive (e.g., below 612 100 nm), their contributions to $\sigma_{sca, 525}$ and especially to $\sigma_{bsca, 525}$ could be amplified 613 upon humidification (Fig. S11b). Besides, the shift of size distribution towards larger 614 accumulation-mode particles could also result in a significant elevation in 615 HBF_{525, RH}/HBF₅₂₅ ratios, especially under the condition of a smaller mode diameter 616 and narrower distribution of ultrafine-mode particles (e.g., during NPF events) (Fig. S16a1-b2 for the theoretical sensitivity tests of Sect. S9 in the supplement). 618 Furthermore, the HBF₅₂₅, RH/HBF₅₂₅ ratio exhibited a significant positive correlation 620 with the real part of complex refractive index (n) of bulk aerosols (Fig. S17), and ntends to increase with the aging process of organic species (Moise et al., 2015; G. Zhao et al., 2021). In this sense, the evolution of both aerosol size distribution pattern and chemical compositions, combined with the heterogeneity in aerosol hygroscopicty, could potentially change particle morphology and optical properties (e.g., complex 624 refractive index and elevated HBF_{525, RH}) particularly during heatwave-influenced 625 NPF_{clean, HW} days, characterized with the smallest aerosol R_{eff} (102.8 \pm 12.4 nm) 626 (Figure. S6), lowest number concentration (1897.0 \pm 680.8 cm⁻³) and fraction (0.20 \pm 0.10) of accumulation mode particles, intensified photooxidation, and a higher 628 SOC/OC ratio. The higher HBF₅₂₅, RH/HBF₅₂₅ ratios increased the HBF-derived $\beta(RH)/\beta(dry)$ levels, in combination of the elevated f(RH), further resulting in the highest $f_{RF}(RH)$ observed during P2 NPF_{clean, HW} events. Given that previously observed HBF_{525, RH} was typically lower than HBF₅₂₅ (Titos et al., 2021; Xia et al., 632 2023; L. Zhang et al., 2015), the mean $f_{RF}(RH)$ results of this study ($f_{RF}(85\%) = 2.05 \pm 1.05$ 0.24) were significantly higher than those observed in the Yangtze River Delta $(f_{RF}(85\%) = 1.5, L. \text{ Zhang et al., } 2015), \text{ the North China Plain } (f_{RF}(80\%) = 1.6 \pm 0.2,$ Xia et al., 2023), and some other regions in the world (Titos et al., 2021, Fig. 6d). It 636 should be noted that the reported $f_{RF}(RH)$ for the UGR site (Spain) was even higher,

608

609

610

611

617

619

621

622

623

627

629

630

631

633

634

635

likely due to the higher R_s and α_s used in the derivation of $f_{RF}(RH)$ in that area (Titos et al., 2021).

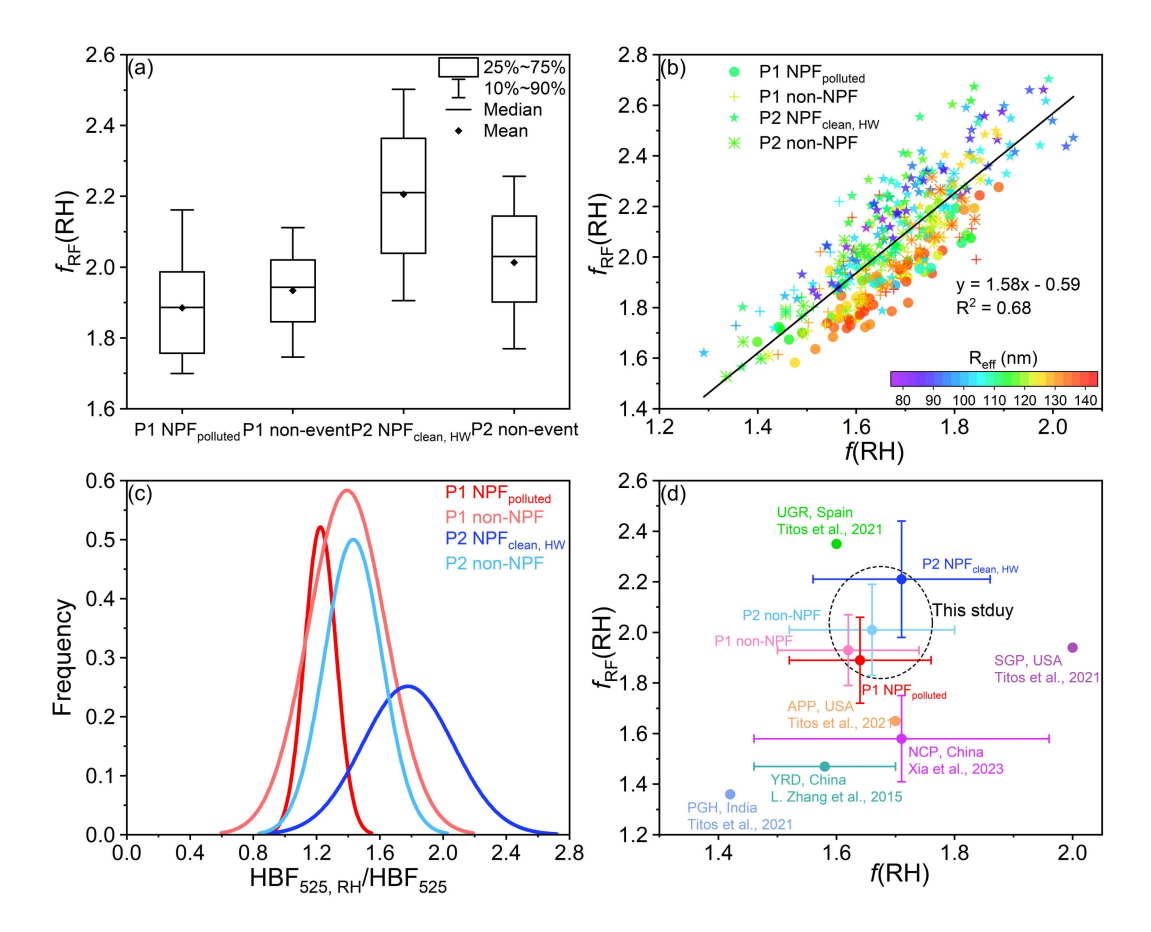


Figure 6. (a) The box-plot of $f_{RF}(RH)$ during P1 or P2 NPF event and non-event days. **(b)** The relationship between $f_{RF}(RH)$ and f(RH), as colored by the corresponding R_{eff} , during P1 or P2 NPF and non-event days (shown in different symbols). **(c)** Occurrence frequency of the HBF₅₂₅, $_{RH}$ /HBF₅₂₅ ratios during P1 or P2 NPF and non-event days. **(d)** The mean $f_{RF}(RH)$ under different f(RH) levels (the error bars stand for \pm one standard deviations corresponding to $f_{RF}(RH)$ and f(RH), respectively), along with the reported $f_{RF}(RH)$ and f(RH) data for other regions in the world.

A recent study has indicated that continuous reduction of PM_{2.5} mass loadings can increase the net solar radiation, thereby promoting NPF events (S. Zhao et al., 2021). Given the complexity and dynamic evolution of the atmospheric environment, these can further alter the intrinsic properties of aerosol particles (e.g., *f*(RH), HBF, morphology), potentially feeding back into aerosol-radiation interactions. Our findings suggest that NPF and growth eventsdays may elevatepossess a relatively

higher aerosol optical hygroscopicity in rather hot environments, e.g., the Basin area and tropical regions. Meanwhile, NPF serves as a crucial secondary transformation process in the atmosphere (Zhu et al., 2021). The favorable atmospheric diffusion capability ensured the mixing of newly formed particles into the upper boundary layer, where is colder and more humid than that near the surface during heatwaves (Jin et al., 2022). Hence, the enhancement of aerosol optical hygroscopicity during the subsequent growth and aging of both pre-existing and newly formed particles possibly exacerbates secondary pollution and even triggers haze events (Hao et al., 2024; Kulmala et al., 2021). On the other hand, a large number of studies have demonstrated that the new particles of higher hygroscopicity could contribute more to the activation of CCN (Ma et al., 2016; Ren et al., 2021; Rosati et al., 2022; Sun et al., 2024; Wu et al., 2015), thereby modulating the aerosol-cloud interactions and further the global climate (Fan et al., 2016; Merikanto et al., 2006; Westervelt et al., 2013). Additionally, the simultaneous decrease aerosol effective radius in and possibly evaporation-induced non-spherical particle morphology further enhance the aerosol direct radiative forcing enhancement factor, potentially amplifying the cooling effect mainly caused by light scattering aerosols. This highlights the needs for further in-depth exploration on aerosol radiative impacts under heatwaves with the changing climate, given the continuous reductions of anthropogenic emissions and more intense emissions of biogenic origins with the global warming. Besides, more detailed information on the evolution of particle morphology with the changing environment (e.g., varied temperature and RH) would enrich insights into the aerosol radiative forcing.

677

678

679

680

681

654

655

656

657

658

659

660

661

662

663

664

665

666

667

668

669

670

671

672

673

674

675

676

4 Conclusions and implications

A rare heatwave event raged throughout urban Chongqing of southwest China in the summer of 2022, which significantly influenced aerosol physicochemical properties and atmospheric processes (e.g., NPF and subsequent growth). Concurrent measurements of aerosol optical and hygroscopic properties, PNSD, and bulk chemical compositions were conducted to explore the mechanisms behind the variations in aerosol optical hygroscopicity during different NPF days under diverse weather conditions.

682

683

684

685

686

687

688

689

690

691

692

693

694

695

696

697

698

699

700

701

702

703

704

705

706

707

708

709

710

Although the air masses and the occurrence frequencies of NPF events were similar during different periods, NPF events exhibited distinct characteristics during the normally hot (P1, relatively polluted) and heatwaves-dominated (P2, quite clean) periods. NPF_{polluted} within P1 period was favored by the decrease in background aerosol loading and the higher abundance of H₂SO₄. NPF_{clean, HW} events that occurred during the heatwave P2 period were observed with lower CS, CoagS, FR and GR, as well as smaller Reff and D_{mode}, than P1 NPF_{polluted} cases. According to the measured PNSDs, the P1 NPF_{polluted} events were mainly driven by local growth, while NPF_{clean, HW} events may be largely affected by transport under heatwaves. In comparison to the P1 NPF_{polluted} events, NPF_{clean, HW} occurred approximately one hour earlier and the subsequent growth was longer during P2, likely intensifying the photochemical oxidation and prolonging atmospheric due to heatwave-influenced aging processes under heatwaves, and thereby modulating the evolution of aerosol size distributions and chemical characteristics differently. Furthermore, significant differences in aerosol optical and hygroscopic properties were observed between the normally hot and heatwave-dominated NPF days. The newly formed and grown particles mixed with pre-existing aerosols contributed a minor $\sigma_{sca, 525}$ noontime peak occurred on the much cleaner P2 NPF_{clean, HW} days, while the σ_{sca, 525} peaked earlier around the morning rush hours on P1 NPFpolluted days. HBF and SAE were significantly higher on P2 NPF_{clean, HW} days, primarily due to the smaller R_{eff} for heatwave-influenced NPF_{clean, HW} cases. f(RH) remained relatively stable during the daytime of NPF days and peaked around 16:00-18:00 LT. Specifically, aerosol optical hygroscopicity tendedwas observed to be higher during the subsequent growth and aging of both pre-existing particles and newly formed ones on P2 NPF_{clean, HW} days than that for P1 NPF_{polluted} days, which aligned with the higher f_W levels.

Compared with non-event cases, the generally higher levels of daily mean f(RH) levels were generally highersuggested that the aerosol optical hygroscopicity was enhanced on NPF days in the 2022 hot summer of urban Chongqing. A significantly positive (negative) correlation between f(RH) and SAE ($\sigma_{sca, 525}$, or rather the pollution level) was observed on NPF days for both periods, accompanied by higher f(RH) and SAE values on NPF_{clean, HW} days. This was likely due to the observed lower FR and GR caused by possible evaporation of both unstable clusters and particle coatings under heatwaves (Bousiotis et al., 2021; Cusack et al., 2013; Deng et al., 2020; Garmash et al., 2024), thereby reducing aerosol sizes (e.g., R_{eff}, D_{mode}) whereas increasing SAE. Moreover, heatwave-influenced stronger photooxidation enhanced the formation of more hygroscopic secondary components during the subsequent growth/aging processes of both pre-existing and newly formed particles on P2 NPF_{clean, HW} days in comparison to that of P1 NPF_{polluted} cases. The aerosol light scattering or volume concentration was mainly contributed by the larger accumulation-mode particles, while more ultrafine particles dominated the size distribution especially for the initial stage of heatwave-influenced NPF_{clean, HW} events, further leading to a lower f(RH) following the NPF occurrence (i.e., $\sim 12:00$ -15:00 LT) in comparison to P1 NPF_{polluted} days. Changes in f(RH) could potentially impact the aerosol direct radiative forcing. A robust positive (negative) correlation existed between $f_{RF}(RH)$ and f(RH) (R_{eff}). Despite a lower $\sigma_{sca, 525}$ during heatwaves, the corresponding mean $f_{RF}(RH)$ was relatively higher and the maximum value of 2.21 ± 0.23 was observed on P2 NPF_{clean, HW} days, associated with the highest f(RH) (1.71 \pm 0.13), smallest R_{eff} (102.8 \pm 12.4 nm), and highest HBF_{525, RH}/HBF₅₂₅ ratios (1.78 \pm 0.29). The above highlights that heatwaves could influence the NPF characteristics (e.g., the evolution in the aerosol size distribution pattern and chemical composition) and atmospheric processing (although with a decreased aerosol Reff and Dmode likely due to evaporation-resulted non-spherical particle morphology under persistently high temperature conditions). Further, variations in the aerosol size distribution and optical hygroscopicity under heatwaves were accompanied with the elevated

711

712

713

714

715

716

717

718

719

720

721

722

723

724

725

726

727

728

729

730

731

732

733

734

735

736

737

738

739

HBF_{525, RH}/HBF₅₂₅ ratios, thereby enhancing aerosol optical hygroscopic growth and potentially reducing the net solar radiation directly especially in hot summer. This study revealed divergent changes in aerosol optical and hygroscopic properties on different NPF days, thereby modulating the aerosol radiative forcing distinctly during a heatwave in summer 2022. A comprehensive understanding of the formation mechanisms of different NPF events (e.g., local formation versus the horizontal or vertical transport) in diverse environment is crucial in the future. The last but not the least, further explorations on detailed molecular-scale characterizations (e.g., molecular structures and compositions of newly and secondary formed particles, as well as particle morphology) and aerosol radiative impacts including the aerosol-cloud interactions of both-heatwaves and other weather extremes with the changing climate are highly recommended.

Data availability. Data will be available upon request.

Author contributions. YH and PL: Methodology, Investigation, Data analysis, Formal analysis, Visualization, Validation, Writing – original draft & editing. YG and ZW: Methodology, Investigation, Formal analysis. MT, YC, HX and WH: Data curation, Methodology. FW and YL: Investigation. YK: Methodology, Data analysis, Writing – review & editing. JC: Conceptualization, Methodology, Funding acquisition, Data curation, Writing – review & editing, Supervision.

Competing interests. The authors declare no competing financial interest.

Acknowledgement. This work was supported by the National Natural Science Foundation of China (No. 42105075), Venture and Innovation Support Program for Chongqing Overseas Returnees (No. cx2021021). We thank Biao Xue for the technical support on the utilization and maintenance of the humidified

- nephelometer system. We also thank Ziqian Wang for the TSP filter sample
- collection and Jiawei Zhou for the corresponding offline chemical analysis.

771

772

References

- 773 An, J., Lu, Y., Huang, D. D., Ding, X., Hu, Q., Yan, R., Qiao, L., Zhou, M., Huang, C.,
- Wang, H., Fu, Q., Yu, F., and Wang, L.: Sectoral Size Resolved Particle Number
- 775 Emissions With Speciation: Emission Profile Based Quantification and a Case Study
- in the Yangtze River Delta Region, China, J. Geophys. Res. Atmos., 1-22,
- 777 https://doi.org/10.1029/2024JD041234, 2024.
- Andrews, E., Sheridan, P. J., Fiebig, M., McComiskey, A., Ogren, J. A., Arnott, P.,
- Covert, D., Elleman, R., Gasparini, R., Collins, D., Jonsson, H., Schmid, B., and
- Wang, J.: Comparison of methods for deriving aerosol asymmetry parameter, J.
- 781 Geophys. Res. Atmos., 111, 1–16, https://doi.org/10.1029/2004JD005734, 2006.
- 782 Asmi, E., Frey, A., Virkkula, A., Ehn, M., Manninen, H. E., Timonen, H.,
- 783 Tolonen-Kivimäki, O., Aurela, M., Hillamo, R., and Kulmala, M.: Hygroscopicity and
- 784 chemical composition of antarctic sub-micrometre aerosol particles and observations
- 785 of new particle formation, Atmos. Chem. Phys., 10, 4253–4271,
- 786 https://doi.org/10.5194/acp-10-4253-2010, 2010.
- 787 Bae, M. S., Lee, T., Schauer, J. J., Park, G., Son, Y. B., Kim, K. H., Cho, S. S., Park,
- 788 S. S., Park, K., and Shon, Z. H.: Chemical Characteristics of Size-Resolved Aerosols
- 789 in Coastal Areas during KORUS-AQ Campaign; Comparison of Ion Neutralization
- 790 Model, Asia-Pacific J. Atmos. Sci., 55, 387–399,
- 791 https://doi.org/10.1007/s13143-018-00099-1, 2019.
- Bousiotis, D., Brean, J., Pope, F. D., Dall'Osto, M., Querol, X., Alastuey, A., Perez,
- 793 N., Petäjä, T., Massling, A., Klenø Nøjgaard, J., Nordstrøm, C., Kouvarakis, G.,
- 794 Vratolis, S., Eleftheriadis, K., Niemi, J. V., Portin, H., Wiedensohler, A., Weinhold,
- 795 K., Merkel, M., Tuch, T., and Harrison, R. M.: The effect of meteorological

- conditions and atmospheric composition in the occurrence and development of new
- particle formation (NPF) events in Europe, Atmos. Chem. Phys., 21, 3345-3370,
- 798 https://doi.org/10.5194/acp-21-3345-2021, 2021.
- 799 Brooke Anderson, G. and Bell, M. L.: Heat waves in the United States: Mortality risk
- during heat waves and effect modification by heat wave characteristics in 43 U.S.
- 801 communities, Environ. Health Perspect., 119, 210–218,
- 802 https://doi.org/10.1289/ehp.1002313, 2011.
- 803 Cai, R., Chandra, I., Yang, D., Yao, L., Fu, Y., Li, X., Lu, Y., Luo, L., Hao, J., Ma, Y.,
- Wang, L., Zheng, J., Seto, T., and Jiang, J.: Estimating the influence of transport on
- aerosol size distributions during new particle formation events, Atmos. Chem. Phys.,
- 806 18, 16587–16599, https://doi.org/10.5194/acp-18-16587-2018, 2018.
- 807 Chen, J., Zhao, C. S., Ma, N., and Yan, P.: Aerosol hygroscopicity parameter derived
- from the light scattering enhancement factor measurements in the North China Plain,
- 809 Atmos. Chem. Phys., 14, 8105–8118, https://doi.org/10.5194/acp-14-8105-2014,
- 810 2014.
- 811 Chen, Q., Mu, Z., Song, W., Wang, Y., Yang, Z., Zhang, L., and Zhang, Y. L.:
- 812 Size-Resolved Characterization of the Chromophores in Atmospheric Particulate
- Matter From a Typical Coal-Burning City in China, J. Geophys. Res. Atmos., 124,
- 814 10546–10563, https://doi.org/10.1029/2019JD031149, 2019.
- 815 Chen, T., Wang, T., Xue, L., and Brasseur, G.: Heatwave exacerbates air pollution in
- 816 China through intertwined climate-energy-environment interactions, Sci. Bull., 69,
- 817 2765–2775, https://doi.org/10.1016/j.scib.2024.05.018, 2024.
- 818 China Meteorological Administration, 2022. China Climate Bulletin 2022.
- https://www.cma.gov.cn/zfxxgk/gknr/qxbg/202303/t20230324 5396394.html.
- Accessed on 23 March 2023. (in Chinese).

- Cho Cheung, H., Chung-Kuang Chou, C., Siu Lan Lee, C., Kuo, W. C., and Chang, S.
- 822 C.: Hygroscopic properties and cloud condensation nuclei activity of atmospheric
- aerosols under the influences of Asian continental outflow and new particle formation
- at a coastal site in eastern Asia, Atmos. Chem. Phys., 20, 5911-5922,
- 825 https://doi.org/10.5194/acp-20-5911-2020, 2020.
- 826 Chylek, P. and Wong, J.: Effect of absorbing aerosols on global radiation budget,
- 827 Geophys. Res. Lett., 22, 929–931, https://doi.org/10.1029/95GL00800, 1995.
- 828 Collaud Coen, M., Weingartner, E., Nyeki, S., Cozic, J., Henning, S., Verheggen, B.,
- Gehrig, R., and Baltensperger, U.: Long-term trend analysis of aerosol variables at the
- 830 high-alpine site Jungfraujoch, J. Geophys. Res. Atmos., 112,
- 831 https://doi.org/10.1029/2006JD007995, 2007.
- 832 Covert, D. S., Charlson, R. J., and Ahlquist, N. C.: A Study of the Relationship of
- 833 Chemical Composition and Humidity to Light Scattering by Aerosols, J. Appl.
- 834 Meteorol., 11, 968–976,
- https://doi.org/10.1175/1520-0450(1972)011<0968:asotro>2.0.co;2, 1972.
- 836 Crumeyrolle, S., Kontkanen, J. S. S., Rose, C., Velazquez Garcia, A., Bourrianne, E.,
- Catalfamo, M., Riffault, V., Tison, E., Ferreira De Brito, J., Visez, N., Ferlay, N.,
- 838 Auriol, F., and Chiapello, I.: Measurement report: Atmospheric new particle
- formation at a peri-urban site in Lille, northern France, Atmos. Chem. Phys., 23,
- 840 183–201, https://doi.org/10.5194/acp-23-183-2023, 2023.
- Cusack, M., Alastuey, A., and Querol, X.: Case studies of new particle formation and
- 842 evaporation processes in the western Mediterranean regional background, Atmos.
- 843 Environ., 81, 651–659, https://doi.org/10.1016/j.atmosenv.2013.09.025, 2013.
- Dada, L., Paasonen, P., Nieminen, T., Buenrostro Mazon, S., Kontkanen, J., Peräkylä,
- O., Lehtipalo, K., Hussein, T., Petäjä, T., Kerminen, V. M., Bäck, J., and Kulmala, M.:
- 846 Long-term analysis of clear-sky new particle formation events and nonevents in

- 847 Hyytiälä, Atmos. Chem. Phys., 17, 6227–6241,
- 848 https://doi.org/10.5194/acp-17-6227-2017, 2017.
- Dal Maso, M., Kulmala, M., Riipinen, I., Wagner, R., Hussein, T., Aalto, P. P., and
- Lehtinen, K. E. J.: Formation and growth of fresh atmospheric aerosols: Eight years
- of aerosol size distribution data from SMEAR II, Hyytiälä, Finland, Boreal Environ.
- 852 Res., 10, 323–336, 2005.
- Delene, D. J. and Ogren, J. A.: Variability of aerosol optical properties at four North
- 854 American surface monitoring sites, J. Atmos. Sci., 59, 1135-1150,
- https://doi.org/10.1175/1520-0469(2002)059<1135:VOAOPA>2.0.CO;2, 2002.
- Deng, C., Cai, R., Yan, C., Zheng, J., and Jiang, J.: Formation and growth of sub-3
- nm particles in megacities: Impact of background aerosols, Faraday Discuss., 226,
- 858 348–363, https://doi.org/10.1039/d0fd00083c, 2021.
- 859 Deng, C., Fu, Y., Dada, L., Yan, C., Cai, R., Yang, D., Zhou, Y., Yin, R., Lu, Y., Li,
- 860 X., Qiao, X., Fan, X., Nie, W., Kontkanen, J., Kangasluoma, J., Chu, B., Ding, A.,
- Kerminen, V. M., Paasonen, P., Worsnop, D. R., Bianchi, F., Liu, Y., Zheng, J., Wang,
- L., Kulmala, M., and Jiang, J.: Seasonal characteristics of new particle formation and
- growth in urban Beijing, Environ. Sci. Technol., 54, 8547–8557,
- 864 https://doi.org/10.1021/acs.est.0c00808, 2020.
- 865 Duan, J., Huang, R. J., Wang, Y., Xu, W., Zhong, H., Lin, C., Huang, W., Gu, Y.,
- 866 Ovadnevaite, J., Ceburnis, D., and O'Dowd, C.: Measurement report: Size-resolved
- secondary organic aerosol formation modulated by aerosol water uptake in wintertime
- haze, Atmos. Chem. Phys., 24, 7687–7698, https://doi.org/10.5194/acp-24-7687-2024,
- 869 2024.
- 870 Fan, J., Wang, Y., Rosenfeld, D., and Liu, X.: Review of aerosol-cloud interactions:
- Mechanisms, significance, and challenges, J. Atmos. Sci., 73, 4221-4252,
- 872 https://doi.org/10.1175/JAS-D-16-0037.1, 2016.

- Fierz-Schmidhauser, R., Zieger, P., Gysel, M., Kammermann, L., Decarlo, P. F.,
- 874 Baltensperger, U., and Weingartner, E.: Measured and predicted aerosol light
- scattering enhancement factors at the high alpine site Jungfraujoch, Atmos. Chem.
- 876 Phys, 10, 2319–2333, 2010.
- 677 Garmash, O., Ezhova, E., Arshinov, M., Belan, B., Lampilahti, A., Davydov, D., Räty,
- M., Aliaga, D., Baalbaki, R., Chan, T., Bianchi, F., Kerminen, V. M., Petäjä, T., and
- Kulmala, M.: Heatwave reveals potential for enhanced aerosol formation in Siberian
- 880 boreal forest, Environ. Res. Lett., 19, https://doi.org/10.1088/1748-9326/ad10d5,
- 881 2024.
- 882 Giordano, M., Espinoza, C., and Asa-Awuku, A.: Experimentally measured
- morphology of biomass burning aerosol and its impacts on CCN ability, Atmos.
- 884 Chem. Phys., 15, 1807–1821, https://doi.org/10.5194/acp-15-1807-2015, 2015.
- 885 Gu, Y., Huang, R. J., Duan, J., Xu, W., Lin, C., Zhong, H., Wang, Y., Ni, H., Liu, Q.,
- 886 Xu, R., Wang, L., and Li, Y. J.: Multiple pathways for the formation of secondary
- organic aerosol in the North China Plain in summer, Atmos. Chem. Phys., 23,
- 888 5419–5433, https://doi.org/10.5194/acp-23-5419-2023, 2023.
- Guenther, A. B., Monson, R. K., and Fall, R.: Isoprene and monoterpene emission
- 890 rate variability: Observations with eucalyptus and emission rate algorithm
- development, J. Geophys. Res. Atmos., 96, 10799–10808,
- 892 https://doi.org/10.1029/91jd00960, 1991.
- 893 Guo, X., Huang, J., Luo, Y., Zhao, Z., and Xu, Y.: Projection of heat waves over
- China for eight different global warming targets using 12 CMIP5 models, Theor. Appl.
- 895 Climatol., 128, 507–522, https://doi.org/10.1007/s00704-015-1718-1, 2016.
- Hamed, A., Joutsensaari, J., Mikkonen, S., Sogacheva, L., Dal Maso, M., Kulmala,
- 897 M., Cavalli, F., Fuzzi, S., Facchini, M. C., Decesari, S., Mircea, M., Lehtinen, K. E. J.,

- and Laaksonen, A.: Nucleation and growth of new particles in Po Valley, Italy, Atmos.
- 899 Chem. Phys., 7, 355–376, https://doi.org/10.5194/acp-7-355-2007, 2007.
- Hamed, A., Korhonen, H., Sihto, S. L., Joutsensaari, J., Jrvinen, H., Petäjä, T., Arnold,
- 901 F., Nieminen, T., Kulmala, M., Smith, J. N., Lehtinen, K. E. J., and Laaksonen, A.:
- The role of relative humidity in continental new particle formation, J. Geophys. Res.
- 903 Atmos., 116, 1–12, https://doi.org/10.1029/2010JD014186, 2011.
- 904 Hand, J. L. and Malm, W. C.: Review of aerosol mass scattering efficiencies from
- 905 ground-based measurements since 1990, J. Geophys. Res. Atmos., 112,
- 906 https://doi.org/10.1029/2007JD008484, 2007.
- Hao, Y., Gou, Y., Wang, Z., Huang, W., Wan, F., Tian, M., and Chen, J.: Current
- on challenges in the visibility improvement of urban Chongqing in Southwest China:
- From the perspective of PM2.5-bound water uptake property over 2015–2021, Atmos.
- 910 Res., 300, 107215, https://doi.org/10.1016/j.atmosres.2023.107215, 2024.
- 911 Hao, Z., Chen, Y., Feng, S., Liao, Z., An, N., and Li, P.: The 2022
- 912 Sichuan-Chongqing spatio-temporally compound extremes: a bitter taste of novel
- 913 hazards, Sci. Bull., 68, 1337–1339, https://doi.org/10.1016/j.scib.2023.05.034, 2023.
- Hauser, M., Orth, R., and Seneviratne, S. I.: Role of soil moisture versus recent
- climate change for the 2010 heat wave in western Russia, Geophys. Res. Lett., 43,
- 916 2819–2826, https://doi.org/10.1002/2016GL068036, 2016.
- Jefferson, A., Hageman, D., Morrow, H., Mei, F., and Watson, T.: Seven years of
- aerosol scattering hygroscopic growth measurements from SGP: Factors influencing
- 919 water uptake, J. Geophys. Res. Atmos., 122, 9451–9466,
- 920 https://doi.org/10.1002/2017JD026804, 2017.
- 921 Jin, X., Li, Z., Wu, T., Wang, Y., Cheng, Y., Su, T., Wei, J., Ren, R., Wu, H., Li, S.,
- 22 Zhang, D., and Cribb, M.: The different sensitivities of aerosol optical properties to
- particle concentration, humidity, and hygroscopicity between the surface level and the

- 924 upper boundary layer in Guangzhou, China, Sci. Total Environ., 803, 150010,
- 925 https://doi.org/10.1016/j.scitotenv.2021.150010, 2022.
- 826 Kerminen, V. M., Chen, X., Vakkari, V., Petäjä, T., Kulmala, M., and Bianchi, F.:
- 927 Atmospheric new particle formation and growth: Review of field observations,
- 928 Environ. Res. Lett., 13, https://doi.org/10.1088/1748-9326/aadf3c, 2018.
- Kim, N., Yum, S. S., Park, M., Park, J. S., Shin, H. J., and Ahn, J. Y.: Hygroscopicity
- of urban aerosols and its link to size-resolved chemical composition during spring and
- 931 summer in Seoul, Korea, Atmos. Chem. Phys., 20, 11245-11262,
- 932 https://doi.org/10.5194/acp-20-11245-2020, 2020.
- 833 Kotchenruther, R. A., Hobbs, P. V., and Hegg, D. A.: Humidification factors for
- atmospheric aerosols off the mid-Atlantic coast of the United States, J. Geophys. Res.
- 935 Atmos., 104, 2239–2251, https://doi.org/10.1029/98JD01751, 1999.
- 936 Kuang, Y., He, Y., Xu, W., Zhao, P., Cheng, Y., Zhao, G., Tao, J., Ma, N., Su, H.,
- 237 Zhang, Y., Sun, J., Cheng, P., Yang, W., Zhang, S., Wu, C., Sun, Y., and Zhao, C.:
- Distinct diurnal variation in organic aerosol hygroscopicity and its relationship with
- 939 oxygenated organic aerosol, Atmos. Chem. Phys., 20, 865-880,
- 940 https://doi.org/10.5194/acp-20-865-2020, 2020.
- 941 Kuang, Y., Zhao, C. S., Zhao, G., Tao, J. C., Xu, W., Ma, N., and Bian, Y. X.: A
- 942 novel method for calculating ambient aerosol liquid water content based on
- measurements of a humidified nephelometer system, Atmos. Meas. Tech., 11,
- 944 2967–2982, https://doi.org/10.5194/amt-11-2967-2018, 2018.
- Kuang, Y., Zhao, C., Tao, J., Bian, Y., Ma, N., and Zhao, G.: A novel method for
- deriving the aerosol hygroscopicity parameter based only on measurements from a
- 947 humidified nephelometer system, Atmos. Chem. Phys., 17, 6651–6662,
- 948 https://doi.org/10.5194/acp-17-6651-2017, 2017.

- Kulmala, M., Dada, L., Daellenbach, K. R., Yan, C., Stolzenburg, D., Kontkanen, J.,
- Ezhova, E., Hakala, S., Tuovinen, S., Kokkonen, T. V., Kurppa, M., Cai, R., Zhou, Y.,
- Yin, R., Baalbaki, R., Chan, T., Chu, B., Deng, C., Fu, Y., Ge, M., He, H., Heikkinen,
- L., Junninen, H., Liu, Y., Lu, Y., Nie, W., Rusanen, A., Vakkari, V., Wang, Y., Yang, G.,
- 953 Yao, L., Zheng, J., Kujansuu, J., Kangasluoma, J., Petaja, T., Paasonen, P., Jarvi, L.,
- Worsnop, D., Ding, A., Liu, Y., Wang, L., Jiang, J., Bianchi, F., and Kerminen, V. M.:
- 955 Is reducing new particle formation a plausible solution to mitigate particulate air
- pollution in Beijing and other Chinese megacities?, Faraday Discuss., 226, 334–347,
- 957 https://doi.org/10.1039/d0fd00078g, 2021.
- Kulmala, M., Petäjä, T., Nieminen, T., Sipilä, M., Manninen, H. E., Lehtipalo, K., Dal
- 959 Maso, M., Aalto, P. P., Junninen, H., Paasonen, P., Riipinen, I., Lehtinen, K. E. J.,
- Laaksonen, A., and Kerminen, V. M.: Measurement of the nucleation of atmospheric
- 961 aerosol particles, Nat. Protoc., 7, 1651–1667, https://doi.org/10.1038/nprot.2012.091,
- 962 2012.
- 963 Kulmala, M.: How Particles Nucleate and Grow, Science, 302, 1000-1001,
- 964 https://doi.org/10.1126/science.1090848, 2003.
- Kurtén, T., Torpo, L., Ding, C. G., Vehkamäki, H., Sundberg, M. R., Laasonen, K.,
- and Kulmala, M.: A density functional study on water-sulfuric acid-ammonia clusters
- and implications for atmospheric cluster formation, J. Geophys. Res. Atmos., 112, 1–7,
- 968 https://doi.org/10.1029/2006JD007391, 2007.
- 969 Lai, S., Hai, S., Gao, Y., Wang, Y., Sheng, L., Lupascu, A., Ding, A., Nie, W., Qi, X.,
- 970 Huang, X., Chi, X., Zhao, C., Zhao, B., Shrivastava, M., Fast, J. D., Yao, X., and Gao,
- 971 H.: The striking effect of vertical mixing in the planetary boundary layer on new
- particle formation in the Yangtze River Delta, Sci. Total Environ., 829, 154607,
- 973 https://doi.org/10.1016/j.scitotenv.2022.154607, 2022.
- Lee, K., Chandra, I., Seto, T., Inomata, Y., Hayashi, M., Takami, A., Yoshino, A., and
- Otani, Y.: Aerial observation of atmospheric nanoparticles on Fukue Island, Japan,

- 976 Aerosol Air Qual. Res., 19, 981–994, https://doi.org/10.4209/aaqr.2018.03.0077,
- 977 2019.
- 278 Li, Y., Ding, Y., and Li, W.: Observed trends in various aspects of compound heat
- 979 waves across China from 1961 to 2015, J. Meteorol. Res., 31, 455–467,
- 980 https://doi.org/10.1007/s13351-017-6150-2, 2017.
- Li, Z., Tikkanen, O. P., Buchholz, A., Hao, L., Kari, E., Yli-Juuti, T., and Virtanen, A.:
- 982 Effect of Decreased Temperature on the Evaporation of α-Pinene Secondary Organic
- 983 Aerosol Particles, ACS Earth Sp. Chem., 3, 2775–2785,
- 984 https://doi.org/10.1021/acsearthspacechem.9b00240, 2019.
- Liu, H. J., Zhao, C. S., Nekat, B., Ma, N., Wiedensohler, A., Van Pinxteren, D.,
- 986 Spindler, G., Müller, K., and Herrmann, H.: Aerosol hygroscopicity derived from
- 987 size-segregated chemical composition and its parameterization in the North China
- 988 Plain, Atmos. Chem. Phys., 14, 2525–2539, https://doi.org/10.5194/acp-14-2525-2014,
- 989 2014.
- Liu, P. F., Zhao, C. S., Göbel, T., Hallbauer, E., Nowak, A., Ran, L., Xu, W. Y., Deng,
- 29. Z. Z., Ma, N., Mildenberger, K., Henning, S., Stratmann, F., and Wiedensohler, A.:
- 992 Hygroscopic properties of aerosol particles at high relative humidity and their diurnal
- variations in the north China plain, Atmos. Chem. Phys., 11, 3479–3494,
- 994 https://doi.org/10.5194/acp-11-3479-2011, 2011.
- 995 Lu, Y., Yan, C., Fu, Y., Chen, Y., Liu, Y., Yang, G., Wang, Y., Bianchi, F., Chu, B.,
- Zhou, Y., Yin, R., Baalbaki, R., Garmash, O., Deng, C., Wang, W., Liu, Y., Petäjä, T.,
- 997 Kerminen, V. M., Jiang, J., Kulmala, M., and Wang, L.: A proxy for atmospheric
- daytime gaseous sulfuric acid concentration in urban Beijing, Atmos. Chem. Phys., 19,
- 999 1971–1983, https://doi.org/10.5194/acp-19-1971-2019, 2019.

- Luoma, K., Virkkula, A., Aalto, P., Petäjä, T., and Kulmala, M.: Over a 10-year record
- of aerosol optical properties at SMEAR II, Atmos. Chem. Phys., 19, 11363-11382,
- 1002 https://doi.org/10.5194/acp-19-11363-2019, 2019.
- 1003 Ma, C. Sen, Ma, G., and Pincebourde, S.: Survive a Warming Climate: Insect
- 1004 Responses to Extreme High Temperatures, Annu. Rev. Entomol., 66, 163–184,
- 1005 https://doi.org/10.1146/annurev-ento-041520-074454, 2021.
- 1006 Ma, N., Zhao, C., Tao, J., Wu, Z., Kecorius, S., Wang, Z., Groß, J., Liu, H., Bian, Y.,
- Kuang, Y., Teich, M., Spindler, G., Muller, K., Van Pinxteren, D., Herrmann, H., Hu,
- 1008 M., and Wiedensohler, A.: Variation of CCN activity during new particle formation
- 1009 events in the North China Plain, Atmos. Chem. Phys., 16, 8593-8607,
- 1010 https://doi.org/10.5194/acp-16-8593-2016, 2016.
- 1011 Marshall, S. F., Covert, D. S., and Charlson, R. J.: Relationship between asymmetry
- parameter and hemispheric backscatter ratio: implications for climate forcing by
- 1013 aerosols, Appl. Opt., 34, 5–6, 1995.
- 1014 Merikanto, J., Spracklen, D. V, Mann, G. W., Pickering, S. J., and Carslaw, K. S.:
- 1015 Atmospheric Chemistry and Physics Impact of nucleation on global CCN, Atmos.
- 1016 Chem. Phys, 9, 8601–8616, 2009.
- 1017 Mishchenko, M. I.: Electromagnetic scattering by nonspherical particles: A tutorial
- 1018 review, J. Quant. Spectrosc. Radiat. Transf., 110, 808-832,
- 1019 https://doi.org/10.1016/j.jqsrt.2008.12.005, 2009.
- 1020 Moise, T., Flores, J. M., and Rudich, Y.: Optical Properties of Secondary Organic
- 1021 Aerosols and Their Changes by Chemical Processes, Chem. Rev., 115, 4400–4439,
- 1022 https://doi.org/10.1021/cr5005259, 2015.
- Nairn, J. R. and Fawcett, R. J. B.: The excess heat factor: A metric for heatwave
- intensity and its use in classifying heatwave severity, Int. J. Environ. Res. Public
- Health, 12, 227–253, https://doi.org/10.3390/ijerph120100227, 2014.

- 1026 Platis, A., Altstädter, B., Wehner, B., Wildmann, N., Lampert, A., Hermann, M.,
- 1027 Birmili, W., and Bange, J.: An Observational Case Study on the Influence of
- 1028 Atmospheric Boundary-Layer Dynamics on New Particle Formation, Boundary-Layer
- 1029 Meteorol., 158, 67–92, https://doi.org/10.1007/s10546-015-0084-y, 2016.
- 1030 Petters, M. D. and Kreidenweis, S. M.: A single parameter representation of
- hygroscopic growth and cloud condensation nucleus activity, Atmos. Chem. Phys., 7,
- 1032 1961–1971, https://doi.org/10.5194/acp-7-1961-2007, 2007.
- 1033 Pierce, T. E. and Waldruff, P. S.: Pc-beis: A personal computer version of the biogenic
- 1034 emissions inventory system, J. Air Waste Manag. Assoc., 41, 937-941,
- 1035 https://doi.org/10.1080/10473289.1991.10466890, 1991.
- 1036 Quinn, P. K., Bates, T. S., Baynard, T., Clarke, A. D., Onasch, T. B., Wang, W., Rood,
- 1037 M. J., Andrews, E., Allan, J., Carrico, C. M., Coffman, D., and Worsnop, D.: Impact
- of particulate organic matter on the relative humidity dependence of light scattering: A
- 1039 simplified parameterization, Geophys. Res. Lett., 32, 1-4,
- 1040 https://doi.org/10.1029/2005GL024322, 2005.
- 1041 Ren, J., Chen, L., Fan, T., Liu, J., Jiang, S., and Zhang, F.: The NPF Effect on CCN
- Number Concentrations: A Review and Re-Evaluation of Observations From 35 Sites
- 1043 Worldwide, Geophys. Res. Lett., 48, 1–12, https://doi.org/10.1029/2021GL095190,
- 1044 2021.
- Rosati, B., Isokääntä, S., Christiansen, S., Jensen, M. M., Moosakutty, S. P., De Jonge,
- 1046 R. W., Massling, A., Glasius, M., Elm, J., Virtanen, A., and Bilde, M.:
- Hygroscopicity and CCN potential of DMS-derived aerosol particles, Atmos. Chem.
- 1048 Phys., 22, 13449–13466, https://doi.org/10.5194/acp-22-13449-2022, 2022.
- Salma, I., Thén, W., Aalto, P., Kerminen, V. M., Kern, A., Barcza, Z., Petäjä, T., and
- Kulmala, M.: Influence of vegetation on occurrence and time distributions of regional

- new aerosol particle formation and growth, Atmos. Chem. Phys., 21, 2861–2880,
- 1052 https://doi.org/10.5194/acp-21-2861-2021, 2021.
- 1053 Schuster, G. L., Dubovik, O., and Holben, B. N.: Angstrom exponent and bimodal
- 1054 aerosol size distributions, J. Geophys. Res. Atmos., 111, 1–14,
- 1055 https://doi.org/10.1029/2005JD006328, 2006.
- 1056 Shang, D., Hu, M., Tang, L., Fang, X., Liu, Y., Wu, Y., Du, Z., Cai, X., Wu, Z., Lou,
- 1057 S., Hallquist, M., Guo, S., and Zhang, Y.: Significant effects of transport on
- nanoparticles during new particle formation events in the atmosphere of Beijing,
- Particuology, 80, 1–10, https://doi.org/10.1016/j.partic.2022.12.006, 2023.
- Sharma, S. and Mujumdar, P.: Increasing frequency and spatial extent of concurrent
- 1061 meteorological droughts and heatwaves in India, Sci. Rep., 7, 1–9,
- 1062 https://doi.org/10.1038/s41598-017-15896-3, 2017.
- Shen, X. J., Sun, J. Y., Zhang, Y. M., Wehner, B., Nowak, A., Tuch, T., Zhang, X. C.,
- Wang, T. T., Zhou, H. G., Zhang, X. L., Dong, F., Birmili, W., and Wiedensohler, A.:
- First long-term study of particle number size distributions and new particle formation
- events of regional aerosol in the North China Plain, Atmos. Chem. Phys., 11,
- 1067 1565–1580, https://doi.org/10.5194/acp-11-1565-2011, 2011.
- Su, Y. W.: The effects of extreme high temperature day off on electricity conservation,
- Weather. Clim. Soc., 13, 769–782, https://doi.org/10.1175/WCAS-D-20-0176.1, 2021.
- Sun, J., Hermann, M., Weinhold, K., Merkel, M., Birmili, W., Yang, Y., Flentje, H.,
- Ries, L., Couret, C., Elsasser, M., Sohmer, R., Wirtz, K., Meinhardt, F., Schü, M.,
- Bath, O., Hellack, B., Kerminen, V., Kulmala, M., Ma, N., and Wiedensohler, A.:
- 1073 Measurement report : Contribution of atmospheric new particle formation to ultrafine
- particle concentration, cloud condensation nuclei and radiative forcing: Results from
- 1075 five-year observations in Central Europe, Atmos. Chem. Phys., 1–34,
- 1076 https://doi.org/10.5194/acp-24-10667-2024, 2024.

- Sun, X., Sun, Q., Zhou, X., Li, X., Yang, M., Yu, A., and Geng, F.: Heat wave impact
- on mortality in Pudong New Area, China in 2013, Sci. Total Environ., 493, 789–794,
- 1079 https://doi.org/10.1016/j.scitotenv.2014.06.042, 2014.
- Sun, Y., Song, L., Yin, H., Zhang, X., Stott, P., Zhou, B., and Hu, T.: 20. Human
- influence on the 2015 extreme high temperature events in Western China, Bull. Am.
- 1082 Meteorol. Soc., 97, S102–S106, https://doi.org/10.1175/BAMS-D-16-0158.1, 2016.
- Tan, J., Zheng, Y., Song, G., Kalkstein, L. S., Kalkstein, A. J., and Tang, X.: Heat
- wave impacts on mortality in Shanghai, 1998 and 2003, Int. J. Biometeorol., 51,
- 1085 193–200, https://doi.org/10.1007/s00484-006-0058-3, 2007.
- Tan, W., Yu, Y., Li, C., Li, J., Kang, L., Dong, H., Zeng, L., and Zhu, T.: Profiling
- 1087 Aerosol Liquid Water Content Using a Polarization Lidar, Environ. Sci. Technol., 54,
- 1088 3129–3137, https://doi.org/10.1021/acs.est.9b07502, 2020.
- 1089 Tang, M., Chan, C. K., Li, Y. J., Su, H., Ma, Q., Wu, Z., Zhang, G., Wang, Z., Ge, M.,
- 1090 Hu, M., He, H., and Wang, X.: A review of experimental techniques for aerosol
- 1091 hygroscopicity studies, Atmos. Chem. Phys., 19, 12631–12686,
- 1092 https://doi.org/10.5194/acp-19-12631-2019, 2019.
- 1093 Tao, L., Zhou, Z., Tao, J., Zhang, L., Wu, C., Li, J., Yue, D., Wu, Z., Zhang, Z., Yuan,
- 1094 Z., Huang, J., and Wang, B.: High contribution of new particle formation to ultrafine
- particles in four seasons in an urban atmosphere in south China, Sci. Total Environ.,
- 1096 889, https://doi.org/10.1016/j.scitotenv.2023.164202, 2023.
- Teng, M., Liao, H., Burke, P. J., Chen, T., and Zhang, C.: Adaptive responses: the
- effects of temperature levels on residential electricity use in China, Clim. Change, 172,
- 1099 https://doi.org/10.1007/s10584-022-03374-3, 2022.
- Tian, J., Wang, Q., Zhang, Y., Yan, M., Liu, H., Zhang, N., Ran, W., and Cao, J.:
- 1101 Impacts of primary emissions and secondary aerosol formation on air pollution in an

- urban area of China during the COVID-19 lockdown, Environ. Int., 150, 106426,
- 1103 https://doi.org/10.1016/j.envint.2021.106426, 2021.
- 1104 Titos, G., Burgos, M. A., Zieger, P., Alados-Arboledas, L., Baltensperger, U.,
- Jefferson, A., Sherman, J., Weingartner, E., Henzing, B., Luoma, K., O'Dowd, C.,
- Wiedensohler, A., and Andrews, E.: A global study of hygroscopicity-driven
- light-scattering enhancement in the context of other in situ aerosol optical properties,
- 1108 Atmos. Chem. Phys., 21, 13031–13050, https://doi.org/10.5194/acp-21-13031-2021,
- 1109 2021.
- 1110 Titos, G., Cazorla, A., Zieger, P., Andrews, E., Lyamani, H., Granados-Muñoz, M. J.,
- Olmo, F. J., and Alados-Arboledas, L.: Effect of hygroscopic growth on the aerosol
- light-scattering coefficient: A review of measurements, techniques and error sources,
- 1113 Atmos. Environ., 141, 494–507, https://doi.org/10.1016/j.atmosenv.2016.07.021,
- 1114 2016.
- 1115 Titos, G., Jefferson, A., Sheridan, P. J., Andrews, E., Lyamani, H., Alados-Arboledas,
- 1116 L., and Ogren, J. A.: Aerosol light-scattering enhancement due to water uptake during
- 1117 the TCAP campaign, Atmos. Chem. Phys., 14, 7031–7043,
- 1118 https://doi.org/10.5194/acp-14-7031-2014, 2014.
- 1119 Tritscher, T., Jurnyi, Z., Martin, M., Chirico, R., Gysel, M., Heringa, M. F., Decarlo,
- 1120 P. F., Sierau, B., Prévt, A. S. H., Weingartner, E., and Baltensperger, U.: Changes of
- hygroscopicity and morphology during ageing of diesel soot, Environ. Res. Lett., 6,
- https://doi.org/10.1088/1748-9326/6/3/034026, 2011.
- 1123 Wang, N., Du, Y., Chen, D., Meng, H., Chen, X., Zhou, L., Shi, G., Zhan, Y., Feng,
- 1124 M., Li, W., Chen, M., Li, Z., and Yang, F.: Spatial disparities of ozone pollution in
- the Sichuan Basin spurred by extreme, hot weather, Atmos. Chem. Phys., 24,
- 3029-3042, https://doi.org/10.5194/acp-24-3029-2024, 2024.

- 1127 Wang, Y., Li, Z., Zhang, R., Jin, X., Xu, W., Fan, X., Wu, H., Zhang, F., Sun, Y., Wang,
- 1128 Q., Cribb, M., and Hu, D.: Distinct Ultrafine- and Accumulation-Mode Particle
- 1129 Properties in Clean and Polluted Urban Environments, Geophys. Res. Lett., 46,
- 1130 10918–10925, https://doi.org/10.1029/2019GL084047, 2019.
- 1131 Wang, Z. B., Hu, M., Sun, J. Y., Wu, Z. J., Yue, D. L., Shen, X. J., Zhang, Y. M., Pei,
- 1132 X. Y., Cheng, Y. F., and Wiedensohler, A.: Characteristics of regional new particle
- formation in urban and regional background environments in the North China Plain,
- 1134 Atmos. Chem. Phys., 13, 12495–12506, https://doi.org/10.5194/acp-13-12495-2013,
- 1135 2013.
- 1136 Wang, Z., Wu, Z., Yue, D., Shang, D., Guo, S., Sun, J., Ding, A., Wang, L., Jiang, J.,
- Guo, H., Gao, J., Cheung, H. C., Morawska, L., Keywood, M., and Hu, M.: New
- particle formation in China: Current knowledge and further directions, Sci. Total
- Environ., 577, 258–266, https://doi.org/10.1016/j.scitotenv.2016.10.177, 2017.
- Westervelt, D. M., Pierce, J. R., Riipinen, I., Trivitayanurak, W., Hamed, A., Kulmala,
- 1141 M., Laaksonen, A., Decesari, S., and Adams, P. J.: Formation and growth of nucleated
- particles into cloud condensation nuclei: Model-measurement comparison, Atmos.
- 1143 Chem. Phys., 13, 7645–7663, https://doi.org/10.5194/acp-13-7645-2013, 2013.
- Wu, Z. J., Poulain, L., Birmili, W., Größ, J., Niedermeier, N., Wang, Z. B., Herrmann,
- 1145 H., and Wiedensohler, A.: Some insights into the condensing vapors driving new
- particle growth to CCN sizes on the basis of hygroscopicity measurements, Atmos.
- 1147 Chem. Phys., 15, 13071–13083, https://doi.org/10.5194/acp-15-13071-2015, 2015.
- Wu, Z. J., Zheng, J., Shang, D. J., Du, Z. F., Wu, Y. S., Zeng, L. M., Wiedensohler, A.,
- and Hu, M.: Particle hygroscopicity and its link to chemical composition in the urban
- atmosphere of Beijing, China, during summertime, Atmos. Chem. Phys., 16,
- 1151 1123–1138, https://doi.org/10.5194/acp-16-1123-2016, 2016.

- 1152 Xia, C., Sun, J., Hu, X., Shen, X., Zhang, Y., Zhang, S., Wang, J., Liu, Q., Lu, J., Liu,
- 1153 S., and Zhang, X.: Effects of hygroscopicity on aerosol optical properties and direct
- radiative forcing in Beijing: Based on two-year observations, Sci. Total Environ., 857,
- 1155 159233, https://doi.org/10.1016/j.scitotenv.2022.159233, 2023.
- 1156 Xu, W. Y., Zhao, C. S., Ran, L., Deng, Z. Z., Liu, P. F., Ma, N., Lin, W. L., Xu, X. B.,
- 1157 Yan, P., He, X., Yu, J., Liang, W. D., and Chen, L. L.: Characteristics of pollutants and
- their correlation to meteorological conditions at a suburban site in the North China
- Plain, Atmos. Chem. Phys., 11, 4353–4369, https://doi.org/10.5194/acp-11-4353-2011,
- 1160 2011.
- 1161 Xu, W., Chen, C., Qiu, Y., Xie, C., Chen, Y., Ma, N., Xu, W., Fu, P., Wang, Z., Pan,
- 1162 X., Zhu, J., Ngcg, N. L., and Sun, Y.: Size-resolved characterization of organic
- aerosol in the North China Plain: New insights from high resolution spectral analysis,
- Environ. Sci. Atmos., 1, 346–358, https://doi.org/10.1039/d1ea00025j, 2021.
- 1165 Xu, W., Kuang, Y., Xu, W., Zhang, Z., Luo, B., Zhang, X., Tao, J., Qiao, H., Liu, L.,
- and Sun, Y.: Hygroscopic growth and activation changed submicron aerosol
- 1167 composition and properties in the North China Plain, Atmos. Chem. Phys., 24,
- 1168 9387–9399, https://doi.org/10.5194/acp-24-9387-2024, 2024.
- 1169 Xue, B., Kuang, Y., Xu, W., and Zhao, P.: Joint increase of aerosol scattering
- efficiency and aerosol hygroscopicity aggravate visibility impairment in the North
- 1171 China Plain, Sci. Total Environ., 839, 141163,
- https://doi.org/10.1016/j.scitotenv.2022.156279, 2022.
- Yang, P., Feng, Q., Hong, G., Kattawar, G. W., Wiscombe, W. J., Mishchenko, M. I.,
- Dubovik, O., Laszlo, I., and Sokolik, I. N.: Modeling of the scattering and radiative
- properties of nonspherical dust-like aerosols, J. Aerosol Sci., 38, 995–1014,
- https://doi.org/10.1016/j.jaerosci.2007.07.001, 2007.

- 1177 Yarragunta, Y., Srivastava, S., Mitra, D., and Chandola, H. C.: Source apportionment
- of carbon monoxide over India: a quantitative analysis using MOZART-4, Environ.
- 1179 Sci. Pollut. Res., 28, 8722–8742, https://doi.org/10.1007/s11356-020-11099-y, 2021.
- 1180 Yuan, L. and Zhao, C.: Quantifying particle-To-particle heterogeneity in aerosol
- 1181 hygroscopicity, Atmos. Chem. Phys., 23, 3195–3205,
- 1182 https://doi.org/10.5194/acp-23-3195-2023, 2023.
- 1183 Zhang, L., Sun, J. Y., Shen, X. J., Zhang, Y. M., Che, H., Ma, Q. L., Zhang, Y. W.,
- Zhang, X. Y., and Ogren, J. A.: Observations of relative humidity effects on aerosol
- light scattering in the Yangtze River Delta of China, Atmos. Chem. Phys., 15,
- 1186 8439–8454, https://doi.org/10.5194/acp-15-8439-2015, 2015.
- Zhang, R., Khalizov, A. F., Pagels, J., Zhang, D., Xue, H., and McMurry, P. H.:
- 1188 Variability in morphology, hygroscopicity, and optical properties of soot aerosols
- during atmospheric processing, Proc. Natl. Acad. Sci. U. S. A., 105, 10291–10296,
- https://doi.org/10.1073/pnas.0804860105, 2008.
- Zhang, R., Khalizov, A., Wang, L., Hu, M., and Xu, W.: Nucleation and growth of
- 1192 nanoparticles in the atmosphere, Chem. Rev., 112, 1957–2011,
- 1193 https://doi.org/10.1021/cr2001756, 2012.
- Zhang, R., Suh, I., Zhao, J., Zhang, D., Fortner, E. C., Tie, X., Molina, L. T., and
- 1195 Molina, M. J.: Atmospheric new particle formation enhanced by organic acids,
- Science (80-.)., 304, 1487–1490, https://doi.org/10.1126/science.1095139, 2004.
- Zhang, R., Wang, G., Guo, S., Zamora, M. L., Ying, Q., Lin, Y., Wang, W., Hu, M.,
- and Wang, Y.: Formation of Urban Fine Particulate Matter, Chem. Rev., 115,
- 3803–3855, https://doi.org/10.1021/acs.chemrev.5b00067, 2015.
- 1200 Zhang, Z., Xu, W., Zeng, S., Liu, Y., Liu, T., Zhang, Y., Du, A., Li, Y., Zhang, N.,
- Wang, J., Aruffo, E., Han, P., Li, J., Wang, Z., and Sun, Y.: Secondary Organic
- 1202 Aerosol Formation from Ambient Air in Summer in Urban Beijing: Contribution of

- 1203 S/IVOCs and Impacts of Heat Waves, Environ. Sci. Technol. Lett.,
- 1204 https://doi.org/10.1021/acs.estlett.4c00415, 2024.
- 1205 Zhao, C., Yu, Y., Kuang, Y., Tao, J., and Zhao, G.: Recent Progress of Aerosol
- 1206 Light-scattering Enhancement Factor Studies in China, Adv. Atmos. Sci., 36,
- 1207 1015–1026, https://doi.org/10.1007/s00376-019-8248-1, 2019.
- 1208 Zhao, G., Hu, M., Fang, X., Tan, T., Xiao, Y., Du, Z., Zheng, J., Shang, D., Wu, Z.,
- 1209 Guo, S., and Zhao, C.: Larger than expected variation range in the real part of the
- refractive index for ambient aerosols in China, Sci. Total Environ., 779, 146443,
- 1211 https://doi.org/10.1016/j.scitotenv.2021.146443, 2021.
- 1212 Zhao, S., Yu, Y., Li, J., Yin, D., Qi, S., and Qin, D.: Response of particle number
- concentrations to the clean air action plan: Lessons from the first long-term aerosol
- measurements in a typical urban valley in western China, Atmos. Chem. Phys., 21,
- 1215 14959–14981, https://doi.org/10.5194/acp-21-14959-2021, 2021.
- 1216 Zhu, Y., Shen, Y., Li, K., Meng, H., Sun, Y., Yao, X., Gao, H., Xue, L., and Wang, W.:
- 1217 Investigation of Particle Number Concentrations and New Particle Formation With
- 1218 Largely Reduced Air Pollutant Emissions at a Coastal Semi-Urban Site in Northern
- 1219 China, J. Geophys. Res. Atmos., 126, 1–20, https://doi.org/10.1029/2021JD035419,
- 1220 2021.
- Zieger, P., Weingartner, E., Henzing, J., Moerman, M., De Leeuw, G., Mikkilä, J., Ehn,
- 1222 M., Petäjä, T., Clémer, K., Van Roozendael, M., Yilmaz, S., Frieß, U., Irie, H., Wagner,
- 1223 T., Shaiganfar, R., Beirle, S., Apituley, A., Wilson, K., and Baltensperger, U.:
- 1224 Comparison of ambient aerosol extinction coefficients obtained from in-situ,
- 1225 MAX-DOAS and LIDAR measurements at Cabauw, Atmos. Chem. Phys., 11,
- 1226 2603–2624, https://doi.org/10.5194/acp-11-2603-2011, 2011.